© 2018. Published by The Company of Biologists Ltd | Journal of Cell Science (2018) 131, jcs216127. doi:10.1242/jcs.216127

RESEARCH ARTICLE

Rab6 promotes insulin receptor and cathepsin trafficking to regulate autophagy induction and activity in *Drosophila*

Carlos I. Ayala[1], Jung Kim[2] and Thomas P. Neufeld[1,*]

ABSTRACT

The self-degradative process of autophagy is important for energy homeostasis and cytoplasmic renewal. This lysosome-mediated pathway is negatively regulated by the target of rapamycin kinase (TOR) under basal conditions, and requires the vesicle trafficking machinery regulated by Rab GTPases. However, the interactions between autophagy, TOR and Rab proteins remain incompletely understood *in vivo*. Here, we identify Rab6 as a critical regulator of the balance between TOR signaling and autolysosome function. Loss of Rab6 causes an accumulation of enlarged autophagic vesicles resulting in part from a failure to deliver lysosomal hydrolases, rendering autolysosomes with a reduced degradative capacity and impaired turnover. Additionally, Rab6-deficient cells are reduced in size and display defective insulin–TOR signaling as a result of mis-sorting and internalization of the insulin receptor. Our findings suggest that Rab6 acts to maintain the reciprocal regulation between autophagy and TOR activity during distinct nutrient states, thereby balancing autophagosome production and turnover to avoid autophagic stress.

KEY WORDS: Autophagy, Vesicular trafficking, Rab6, Target of rapamycin, *Drosophila*, Insulin, Cathepsin

INTRODUCTION

Autophagy is a catabolic housekeeping mechanism employed by cells to maintain quality control of proteins and organelles. This process can be induced to high levels upon a variety of cellular stressors, such as starvation and loss of target of rapamycin kinase (TOR) activity, and has been shown to regulate a diverse number of developmental processes in higher eukaryotes (Lippai and Szatmári, 2017). Not surprisingly, dysregulation of autophagy is associated with disease states ranging from cancer to neurodegeneration (Jiang and Mizushima, 2014). Canonical macroautophagy, hereafter called autophagy, starts via the formation of an isolation membrane at the endoplasmic reticulum (ER) around cytoplasmic material to be degraded. Extension of the isolation membrane is supported by contribution of membrane sources from endosomes, the Golgi and the plasma membrane, culminating in its closure to produce a double-membrane autophagosome. Afterwards, autophagosomes continue in a maturation path to encounter endosomes and lysosomes to form autolysosomes. Enclosed cargo inside autolysosomes is degraded by lysosomal hydrolases to produce reusable macromolecular building blocks to achieve protein and organelle quality control in the cell and to re-activate TOR at the lysosomal surface (Chen and Yu, 2017; Lippai and Szatmári, 2017).

Vesicular trafficking, the directed movement of vesicles between organelles and other cellular compartments, is an essential aspect of autophagy. The Rab family of proteins, 33 in *Drosophila* and over 60 in mammals, are small lipidated G proteins with key roles in regulating vesicular trafficking (Hutagalung and Novick, 2011; Zhang et al., 2007). Their function is executed in a nucleotide-dependent manner via recruitment of effector proteins and tethering of molecules to promote fusion and fission at organelle surfaces (Stenmark, 2009). Rab GTPases have been shown to regulate anterograde and retrograde trafficking between the ER and Golgi, endosomal to lysosomal maturation and protein secretion among other cellular tasks (Stenmark, 2009). Given the exquisite and specific role of these GTPases in cellular trafficking, it is not surprising that their function is required for proper development and signaling in organisms ranging from yeast to mammals. Much of the research on Rab-mediated trafficking has been focused on the secretory and endosome/lysosome pathways (Hutagalung and Novick, 2011), and a potential role for Rab-mediated trafficking in other cellular pathways, such as autophagy and insulin–TOR signaling remains incompletely understood.

The role of Rab GTPases in the regulation of autophagy has begun to emerge in recent years in yeast and mammalian cell culture, revealing that a small subset of the Rab GTPases regulates this process at different stages (Ao et al., 2014). At the beginning steps, Rab1 and Rab32 are required for isolation membrane synthesis, while Rab5 is required to promote activation of class III PI3K leading to autophagy induction (Hirota and Tanaka, 2009; Ravikumar et al., 2008; Zoppino et al., 2010). Rab11 has been associated with autophagy at two distinct steps, first regulating autophagosome formation and secondly for fusion of maturing autophagosomes with multivesicular bodies (Fader et al., 2008; Longatti et al., 2012). At the last step, Rab7 and Rab14 have been shown to be required for fusion of late endosomes/lysosomes with mature autophagosomes to allow termination of the process and cargo degradation (Gutierrez et al., 2004; Jager et al., 2004; Mauvezin et al., 2016). As most of this work has been performed in yeast and mammalian systems, we decided to study the role Rab GTPases may play in autophagy regulation using, as a model system, the fruit fly *Drosophila melanogaster*. This system has a lower redundancy of family proteins than mammalian cells and provides the complexity of multicellular signaling not attainable with yeast.

Here, we describe the identification of Rab6 as a novel regulator of autophagy and insulin–TOR signaling in *D. melanogaster*. Rab6 is a Golgi-associated protein with well-characterized roles in retrograde transport within the Golgi apparatus and between the Golgi and ER or endosomal membranes (Goud et al., 1990; Luo and Gallwitz, 2003; Martinez et al., 1994; White et al., 1999). It also functions in apical-basal sorting and in cell cycle regulation (Iwanami et al., 2016; Miserey-Lenkei et al., 2006, 2007). The Rab6

[1]Department of Genetics, Cell Biology and Development, 6-160 Jackson Hall, 321 Church St. SE, University of Minnesota, Minneapolis, MN 55455, USA. [2]Department of Molecular and Cell Biology, University of California at Berkeley, Berkeley, CA 94720, USA.

*Author for correspondence (neufe003@umn.edu)

T.P.N., 0000-0001-5659-4811

Received 26 January 2018; Accepted 2 August 2018

Journal of Cell Science (2018) 131, jcs216127. doi:10.1242/jcs.216127

ortholog Ypt6 has been shown to be required for autophagy under stress conditions in yeast, in part by promoting delivery of the membrane protein Atg9 to the autophagosome (Ohashi and Munro, 2010; Yang and Rosenwald, 2016; Ye et al., 2014). To date no role for Rab6 in this process has been described in higher eukaryotes. In this study, we show that loss of Rab6 in the *Drosophila* fat body causes an accumulation of autophagosomes, reduction in cell size and expansion of the lysosomal compartment. Characterization of these phenotypes revealed a mis-sorting of Cathepsin D from lysosomes, rendering them with a reduced degradative capacity upon autophagosome–lysosome fusion. This autolysosomal dysfunction is paired with a defective recovery of TOR activity upon re-feeding. Interestingly, these defects can be rescued by inactivation of the TOR inhibitor PTEN or overexpression of Rheb, but not by re-feeding of exogenous nutrients nor constitutive activation of amino acid signaling, indicating an additional novel role for Rab6 in regulation of the TOR signaling axis. Evaluation of the level of insulin receptor (InR) following nutrient re-feeding after starvation revealed that InR recycling to the plasma membrane is compromised and alternatively mis-routed to the lysosome upon Rab6 loss. Our findings suggest that Rab6 ensures an appropriate balance between autophagy and TOR signaling by affecting two distinct trafficking routes.

RESULTS

Rab6 loss results in accumulation of autolysosomes

In an attempt to identify novel regulators of autophagy, we used the UAS/Gal4 bipartite system to express RNAi transgenes targeting 31 of the 33 Rab GTPases encoded in the *Drosophila* genome. The well-described reporter mCherry–Atg8a was used as a marker to monitor autophagic vesicles (autophagosomes and autolysosomes) in the *Drosophila* larval fat body (Mauvezin et al., 2014). In addition to Rab proteins with previously described functions in autophagy, we found that depletion of Rab6 resulted in an accumulation of mCherry–Atg8a-marked vesicles under fed conditions and an enlargement of these vesicles relative to controls under starvation conditions (Fig. S1A,B; the efficiency of Rab6 depletion is shown in Fig. S1C). Rab6 previously has been shown to regulate protein secretion and endosome-to-Golgi trafficking (Luo and Gallwitz, 2003), but not autophagy. We confirmed and extended these results using a null allele, $Rab6^{D23D}$, monitoring autophagy through mosaic analysis in fat body cell clones (Purcell and Artavanis-Tsakonas, 1999). Clonal loss of Rab6 resulted in a cell-autonomous accumulation of autophagic vesicles; this was observed both in confocal sections through the nuclear plane and at cortical regions of the cell (Fig. 1A,B). Interestingly, accumulation of autophagic vesicles was not observed in Rab6

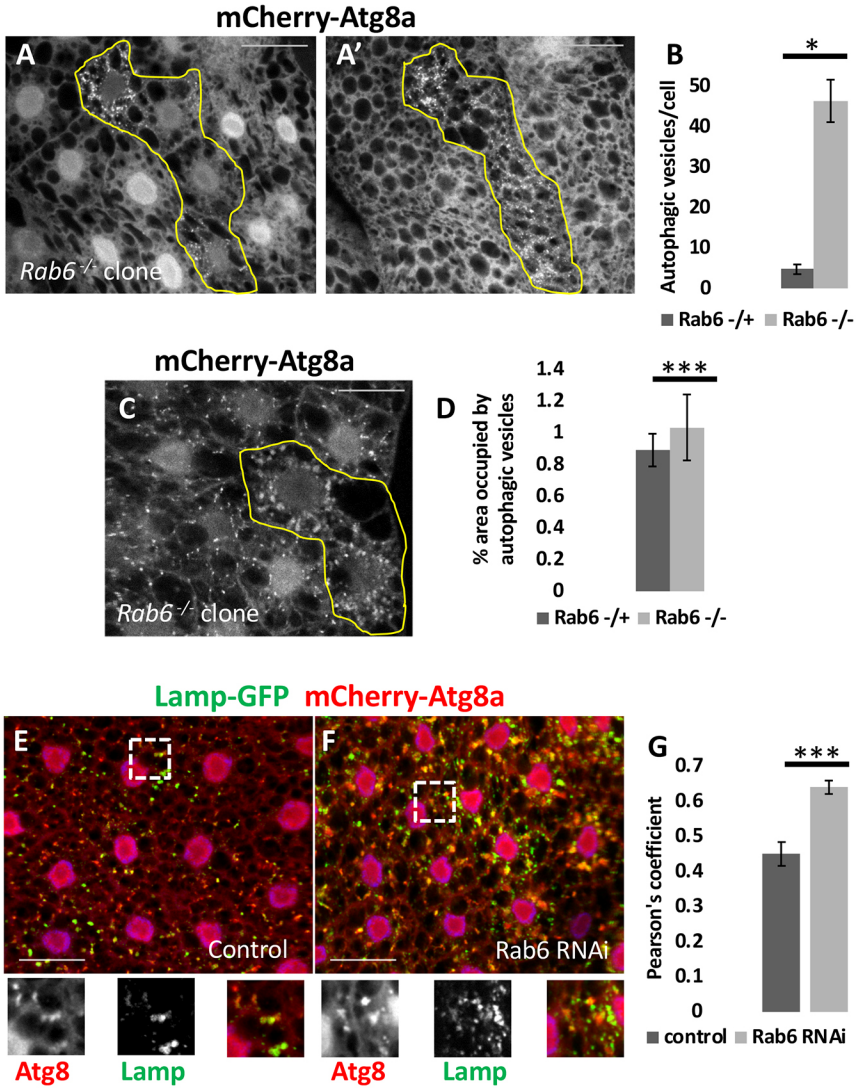

Fig. 1. Loss of Rab6 leads to accumulation of autolysosomes. (A,B) Representative images of larval fat body containing a *Rab6*-null cell clone (outlined in yellow), showing increased accumulation of mCherry–Atg8a-marked autophagic vesicles relative to surrounding control cells under fed conditions. Nuclear (A) and cortical (A′) focal planes are shown. The mean number of mCherry–Atg8a puncta per cell is indicated in (B) for nuclear confocal sections. (C,D) Formation of autophagic vesicles is observed in response to a 4 h starvation in both $Rab6^{-/-}$ cell clones and surrounding control (+/–) cells. The relative area of mCherry–Atg8a puncta is quantified in D. (E–G) mCherry–Atg8a puncta colocalize with Lamp–GFP in both control (E) and Rab6-depleted cells (F) after 4 h in starvation conditions. Colocalization coefficient of these markers is shown in G. *n* values: B, 10 larvae, 60 total clones; D, 10 larvae, 171 total clones; G, 8 larvae, 120 cells per genotype. **P*<0.05, ****P*<0.01 (Student's *t*-test). Error bars indicate s.e.m. Genotypes: A–C, *hs-flp; Rab6*^{D23D}*, FRT40A/UAS-2x-eGFP, FRT40A, fb-Gal4; UAS-mCherry-Atg8a/+*; E, *Cg-Gal4 UAS-Lamp-GFP, UAS-mCherry-Atg8a/+*; F, *Cg-Gal4 UAS-Lamp-GFP, UAS-mCherry-Atg8a/UAS-Rab6-dsRNA*. Scale bars: 25 µm.

Journal of Cell Science (2018) 131, jcs216127. doi:10.1242/jcs.216127

mutant cells in early L3 larvae, suggesting a time-dependent or threshold effect for the observed phenotypes (Fig. S1D). As observed in Rab6-depleted cells, autophagic vesicle size was increased ∼1.5 fold in a subset of the *Rab6*-null cells analyzed (50/171 clonal cells; Fig. 1C,D). Thus, depletion or mutation of Rab6 results in the accumulation of enlarged autophagic vesicles.

Accumulation of autophagic vesicles can arise from a block of fusion between autophagosomes and lysosomes en route to form an autolysosome (Mauvezin et al., 2015). To test for a potential requirement for Rab6 in autophagosome–lysosome fusion, we co-expressed mCherry–Atg8a with the endo-lysosomal markers Lamp–GFP and Rab7–GFP in control and Rab6-depleted cells. The majority of mCherry–Atg8a puncta colocalized with these markers in both cases (Fig. 1E–G; Fig. S1E,F), indicating that loss of Rab6 does not impair autolysosome formation. Together, these results suggest that loss of Rab6 results in the accumulation of autolysosomes.

Lysosomal function is reduced in the absence of Rab6

Defects in lysosomal function can lead to an imbalance between autophagic vesicle production and turnover, a phenomenon described as autophagic stress that is associated with accumulation of enlarged autolysosomes (Chu, 2006; Walls et al., 2007). Consistent with an altered lysosomal function, depletion or mutation of Rab6 led to an expansion of the LAMP-positive lysosomal compartment as compared to control tissue (Fig. 2A–C; Fig. S1G). Staining with Lysotracker, which labels acidified compartments, revealed normal lysosomal acidification in Rab6 depleted cells (Fig. S1H). Accordingly, v-ATPase subunits responsible for lysosomal acidification localized normally to autolysosomes in control and Rab6-depleted cells (Fig. S2A–D) despite a clear enlargement of these vesicles upon Rab6 depletion.

To test the effect of Rab6 on the degradative capacity of autolysosomes, we monitored the autophagic substrate Ref(2)p, using a GFP–Ref(2)P fusion whose levels and degradation can be assayed by immunoblotting with a GFP antibody (Mauvezin et al., 2014). Under fed conditions, basal levels of full-length GFP–Ref(2)p were elevated in extracts of Rab6-depleted fat bodies, as compared to control (Fig. 2D). In addition, production of the free GFP species resulting from starvation-induced autophagic degradation was reduced in Rab6-depleted extracts (Fig. 2D). We also noted higher levels of Ref2p–GFP partial degradation products when Rab6 was depleted. Taken together, these results demonstrate that loss of Rab6 results in expansion of the lysosomal compartment and impairment of autolysosomal function.

In yeast and mammalian cell culture studies, Rab6 has been shown to indirectly control the delivery of hydrolases to the lysosome by regulating retrieval of the hydrolase receptor (M6PR in mammals) from late endosomes/lysosomes via a retrograde endosome-to-Golgi route (Liewen et al., 2005; Medigeshi and Schu, 2003; Siniossoglou and Pelham, 2001). As this could potentially account for the reduced Ref(2)p degradation observed in Rab6-depleted fat body cells, we asked whether lysosomal Cathepsins were delivered to lysosomes in a Rab6-dependent manner. In control cells, antibodies against endogenous Cathepsin-D and -L primarily stained LAMP–GFP-labeled lysosomes (tests for antibody specificity are shown in Fig. S3A–C). Depletion or null mutation of Rab6 led to a loss of Cathepsin staining at these structures, despite an increase in lysosomal size (Fig. 2E,F; Fig. S3D; data not shown). In contrast, depletion of Rab6 had no effect on the localization of GFP-tagged Lysosomal Enzyme Receptor Protein (LERP) (Fig. S4A,B), an ortholog of mammalian M6PR (Dennes et al., 2005). Recently,

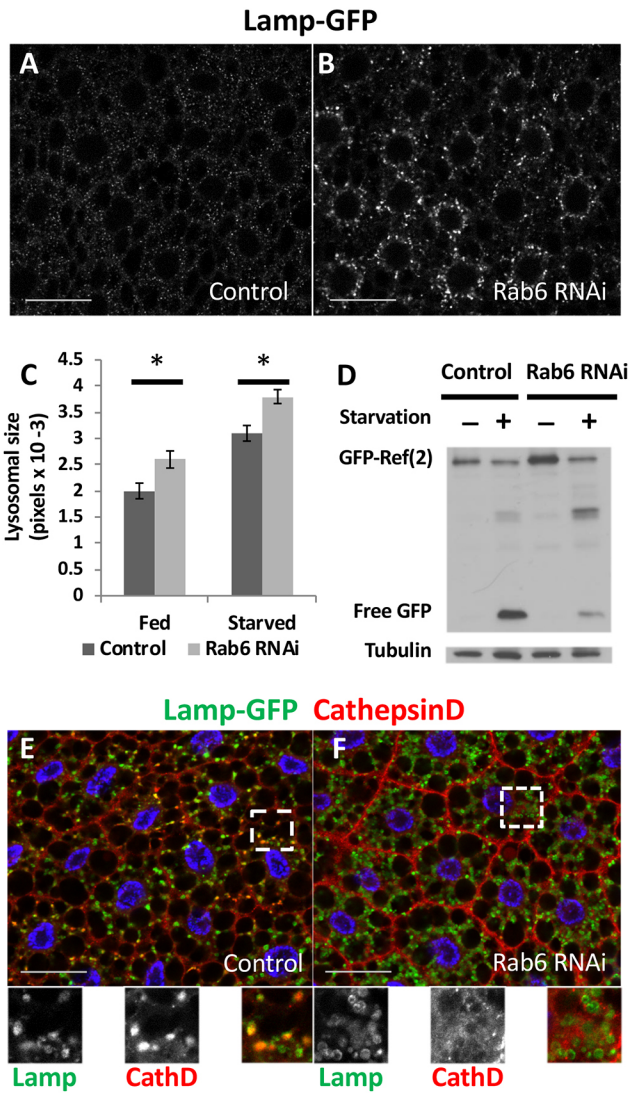

Fig. 2. Rab6 loss results in expansion of the lysosomal compartment and reduced lysosomal function. (A–C) Depletion of Rab6 throughout the larval fat body results in expansion of the Lamp–GFP-marked lysosomal compartment (B) compared to control tissue (A) under fed conditions; data are quantified in C. n=10 larvae, 150 clones per genotype and condition. *P<0.05, ***P<0.01 (Student's t-test). Error bars indicate s.e.m. (D) Rab6 depletion results in higher basal level of GFP–Ref(2)p under fed conditions (lane 3) and reduced degradation under starvation conditions (lane 4), as indicated by generation of free GFP. Fat body extracts from fed and starved larvae expressing UAS-GFP–Ref(2)p were used to detect GFP–Ref(2)p and/or free GFP via western blotting using an anti-GFP antibody. (E,F) Cathepsin D colocalizes with the lysosomal marker Lamp–GFP in control fat body cells but staining is reduced upon Rab6 depletion. The images below show an increased magnification of the indicated region with mCherry–Atg8a (left), LAMP–GFP (middle) and merge (right). 4 h starvation conditions. Scale bars: 25 µm. Genotypes: A,E, *Cg-Gal4 UAS-Lamp-GFP/+*; B,F, *Cg-Gal4 UAS-Lamp-GFP/ UAS-Rab6-dsRNA;* D, control, *r4-GAL4 UAS-Ref(2)p-GFP/+*; Rab6 RNAi, *r4-GAL4 UAS-Ref(2)p-GFP/UAS-Rab6-dsRNA*. Scale bars: 25 µm.

hydrolase sorting in the *Drosophila* larval fat body was shown to occur through a retromer-dependent pathway that is largely independent of LERP (Maruzs et al., 2015). Similarly, our data suggest that Rab6 is required for LERP-independent sorting of hydrolases to ensure lysosomal and autolysosomal function.

To further characterize the role of Rab6 in the sorting of hydrolases, we examined its subcellular distribution (Fig. S4C).

Journal of Cell Science (2018) 131, jcs216127. doi:10.1242/jcs.216127

Sub-populations of YFP–Rab6 colocalized with markers for the Golgi (RFP–Golgi) and lysosome (HRP–LAMP) (Fig. S4D,E). Additionally, under starvation conditions YFP–Rab6 strongly colocalized with mCherry–Atg8a-marked autophagic vesicles (Fig. S4F). Taken together, our data show that Rab6 promotes lysosomal function, potentially through a direct regulatory role in hydrolase sorting.

Rab6 is required for turnover of autophagic vesicles and TOR reactivation

Following the formation of autolysosomes in response to autophagy induction, return to a basal state requires the turnover of these vesicles and reformation of primary lysosomes. This recycling process requires the reactivation of TOR, whose kinase activity is reduced in response to many autophagic stimuli (Chen and Yu, 2017; Yu et al., 2011). To test whether the autophagic vesicles accumulating in Rab6 mutants can be properly recycled, we subjected larvae containing *Rab6*-null clones to 4 h starvation and then transferred them back to rich food for 7 h. In neighboring control cells, both the number and size of mCherry–Atg8a-marked vesicles was markedly reduced in response to re-feeding (Fig. 3A,C). In contrast, these structures remained abundant and enlarged after 7 h on rich food in Rab6 mutant cells (Fig. 3B,C), indicating a defect in autolysosomal turnover. Consistent with these results, depletion of Rab6 led to reduced TOR activity both under basal conditions and in response to re-feeding, as assayed by phosphorylation of the TOR target S6K T398 in larval fat body extracts (Fig. 3D,E). Together, these results suggest that Rab6 promotes autolysosomal homeostasis through at least two mechanisms: (1) by promoting hydrolase delivery and/or sorting, and therefore being required for normal autolysosomal function; and (2) by promoting TOR activity, and hence stimulating autolysosomal reformation and inhibiting formation of new autophagosomes. Reductions in each of these activities likely contribute to the accumulation of enlarged autolysosomes observed in cells lacking Rab6.

Rab6 is required for canonical insulin signaling

Amino acid and insulin signaling are upstream activators of TOR (Shimobayashi and Hall, 2014), and a defect in either of these inputs could potentially explain the reduced TOR activity in cells lacking Rab6. To distinguish between these possibilities, we attempted to rescue Rab6-null mutant phenotypes by activating either amino acid or insulin signaling upstream of TOR. In control fat body clones mutant for Rab6, the autolysosomal compartment was significantly expanded under both fed and starved conditions, as described above (Fig. 4A,D; quantified in Fig. 4I,J). In addition, loss of Rab6 led to a significant reduction in average cell size, consistent with decreased TOR activity of these cells (Fig. 4G,H). Neither of these phenotypes was alleviated by expression of a constitutively active form of RagA, a nutrient-sensitive GTPase that mediates amino acid signaling upstream of TOR (Kim et al., 2008; Sancak et al., 2008) (Fig. 4B,E,I,J). In contrast, overexpression of the GTPase Rheb, a mediator of insulin signaling, fully rescued both the size reduction and autolysosome accumulation of Rab6 mutant cells under starvation conditions, with more modest effects observed in fed animals (Fig. 4C,F,G–J). These genetic epistasis results suggest that Rheb-dependent insulin signaling becomes limiting for TOR activation in Rab6 mutant cells, and they demonstrate that reduced TOR signaling contributes in part to the defective autolysosome dynamics in these cells.

The ability of Rheb overexpression to rescue Rab6 mutant phenotypes suggests that insulin signaling is deficient in these cells. As a more specific readout of this pathway, we monitored the phosphorylation of Akt1 on Ser505 (p-Akt), an established marker of insulin/PI3K activity (Scanga et al., 2001). In fat body extracts of control larvae, p-Akt levels decreased in response to starvation and recovered upon re-feeding (Fig. 5A,B). In Rab6-depleted samples, p-Akt levels were lower than controls under basal conditions, and they failed to recover in response to re-feeding, a pattern similar to that of phosphorylation of S6K (p-S6K). These results show that Rab6 is required for nutrient-dependent activation of Akt.

The phosphatase and tensin homolog (PTEN) is a negative regulator of insulin signaling, opposing activation of Akt and the enhanced PI3P synthesis resulting from insulin binding to its receptor (Worby and Dixon, 2014). In *Drosophila*, mutation of PTEN causes constitutive activation of insulin signaling, leading to cell enlargement and suppression of autophagy (Gao et al., 2000; Goberdhan et al., 1999) (Fig. 5D,F,G). In *Rab6*$^{-/-}$ *Pten*$^{-/-}$ double

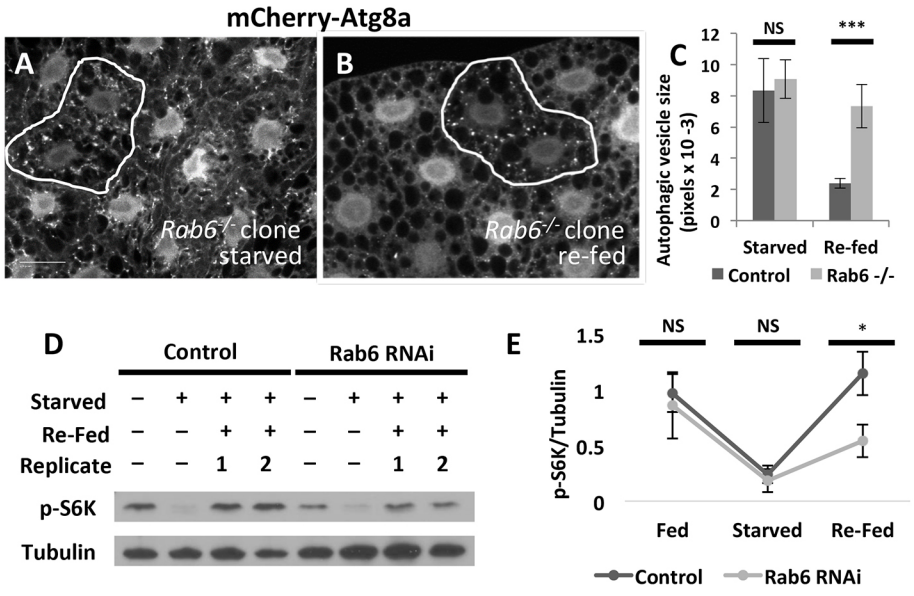

Fig. 3. Nutrient sensing and autophagic clearance are compromised in the absence of Rab6. (A–C) Clones of *Rab6*-null fat body cells (encircled in white) show impaired clearance of autophagic vesicles relative to surrounding control cells upon transition from 4 h starvation conditions (A) to 7 h re-feeding on full (rich) food (B). Scale bar: 25 µm. Autophagic vesicle size is quantified in C. 3.8 pixels per micron. *n*=7 larvae and 13 clones analyzed per genotype and condition. ***P<0.01; NS, not significant (Student's *t*-test). Error bars indicate s.e.m. (D,E) Rab6 depletion results in decreased activation of mTOR upon nutrient re-addition. Fat body extracts from larvae at the indicated time points and nutritional states were used to monitor phosphorylation of S6 kinase. (E) Quantification of data represented in D. Genotypes: A,B, *hs-flp; Rab6*^{D23D}*, FRT40A/UAS-2xeGFP, FRT40A, fb-Gal4; UAS-mCherry-Atg8a/+*; D,E, control, *Cg-Gal4/+*; Rab6 RNAi, *Cg-Gal4/UAS-Rab6-dsRNA*.

Journal of Cell Science (2018) 131, jcs216127. doi:10.1242/jcs.216127

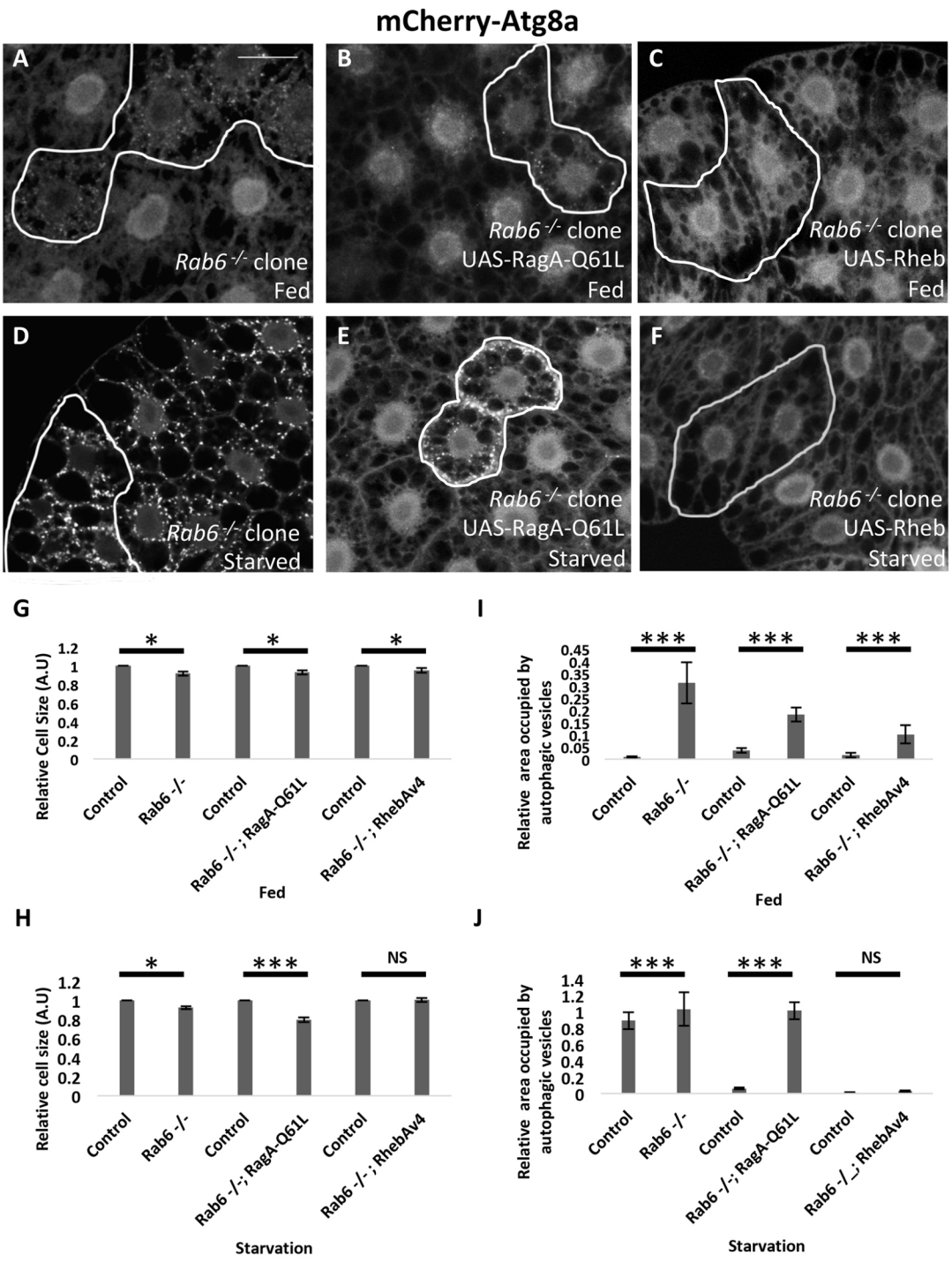

Fig. 4. *Rab6* mutant phenotypes are rescued by overexpression of Rheb, but not by constitutive activation of RagA. (A–F) *Rab6*-null mutant cell clones (outlined in white) were induced in control background (A,D) or in the presence of fat body-specific expression of $RagA^{Q61L}$ (B,E) or wild-type Rheb (C,F), and observed under fed or 4 h starvation conditions. Autophagic vesicles are marked by mCherry–Atg8a. Scale bar: 25 µm. (G–J) Quantification of cell size (G,H) and autophagic vesicle area (I,J) under fed and 4 h starvation conditions for genotypes indicated in A–F. Relative cell size indicates the ratio of the mean cell area within a clone to that of surrounding control cells. Relative area occupied by autophagic vesicles indicates the fraction of cell area occupied by mCherry–Atg8a puncta normalized to starved control cells. Clones analyzed per genotype: A, *n*=60; B, *n*=171; C, *n*=77; D, *n*=56; E, *n*=71; F, *n*=77. A total of 10 larvae per genotype and condition were used for analysis. **P*<0.05; NS, not significant; ****P*<0.01 (Student's *t*-test). Error bars indicate s.e.m. Genotypes: A,D, *hs-flp; Rab6^{D23D}, FRT40A/UAS-2x-eGFP, FRT40A, fb-Gal4; UAS-mCherry-Atg8a/+*; B,E, *hs-flp; Rab6^{D23D}, FRT40A/UAS-2x-eGFP, FRT40A, fb-Gal4; UAS-mCherry-Atg8a/UAS-RagA-Q61L*; C,F, *hs-flp; Rab6^{D23D}, FRT40A/UAS-2x-eGFP, FRT40A, fb-Gal4; UAS-mCherry-Atg8a/UAS-Rheb-AV4*.

mutant cells, the cell size reduction and autolysosome expansion of Rab6 mutants was fully suppressed by loss of PTEN under starvation conditions (Fig. 5E–G) and partially suppressed under basal conditions (Fig. S5). Taken together, these results show that Rab6 is required for normal insulin signaling, and they identify the insulin pathway as playing a causal role in Rab6 functions.

Journal of Cell Science (2018) 131, jcs216127. doi:10.1242/jcs.216127

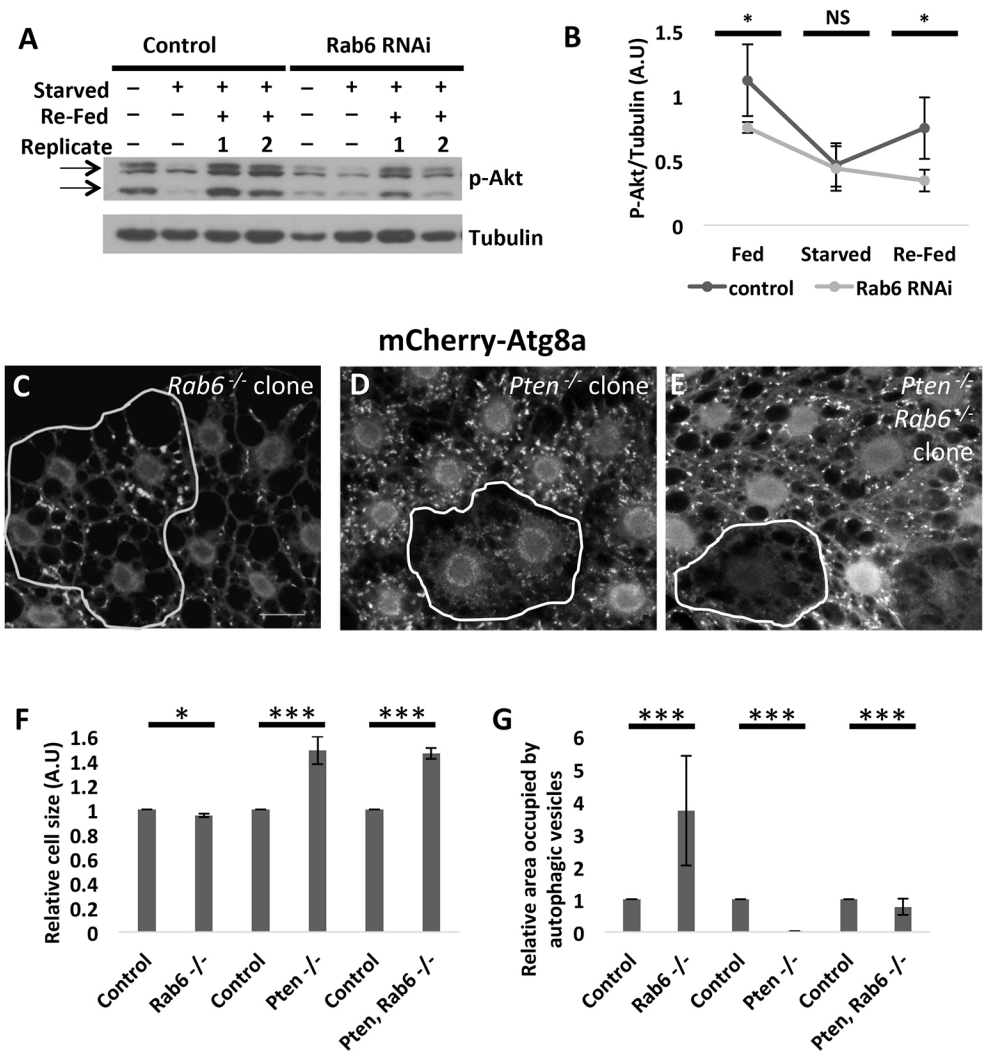

Fig. 5. Loss of Rab6 is rescued by Pten deficiency. (A,B) Akt S505 phosphorylation (p-Akt; arrows indicate two isoforms) is reduced in extracts of Rab6-depleted fat body tissue under basal conditions and in response to re-feeding. A quantification is shown in B. (C–G) Accumulation of mCherry–Atg8a-marked autophagic vesicles in response to 4 h starvation in surrounding control cells and in *Rab6*$^{-/-}$ (C), *Pten*$^{-/-}$ (D), and *Rab6*$^{-/-}$ *Pten*$^{-/-}$ mutant clones. Relative cell size and area occupied by mCherry–Atg8a (each normalized to surrounding control cells) are indicated for the genotypes shown in in C–E. Scale bar: 25 µm. Clones analyzed per genotype: C, *n*=171; D, *n*=15; E, *n*=65. A total of 10 larvae per genotype and condition were analyzed. **P*<0.05, ****P*<0.01; NS, not significant (Student's *t*-test). Error bars indicate s.e.m. Genotypes: A,B, control, *Cg-Gal4/+*; Rab6 RNAi, *Cg-Gal4/UAS-Rab6-dsRNA*; C, *hs-flp; Rab6*^{D23D}*, FRT40A/UAS-2x-eGFP, FRT40A, fb-Gal4; UAS-mCherry-Atg8a/+*; D, *hs-flp; Pten*^{Dj189}*, FRT40A/UAS-2x-eGFP, FRT40A, fb-Gal4; UAS-mCherry-Atg8a/+*; E, *hs-flp; Rab6*^{D23D} *Pten*^{Dj189}*, FRT40A/UAS-2x-eGFP, FRT40A, fb-Gal4; UAS-mCherry-Atg8a/+*.

Rab6 promotes localization of the insulin receptor to the plasma membrane

Insulin signaling is initiated via contact of insulin with the insulin receptor tyrosine kinase (InR) at the plasma membrane. Upon ligation and receptor activation, both insulin and InR are internalized by endocytosis, and InR is recycled from the endocytic compartment back to the plasma membrane (Foti et al., 2004; Goh and Sorkin, 2013). The observation that Rab6 acts upstream of Akt and Pten is consistent with a potential role in InR uptake or trafficking. This prompted us to evaluate the localization of the InR under fed, starved and re-fed conditions in wild-type and Rab6-depleted cells. In control fat body tissues co-expressing fluorescently tagged InR–CFP and LAMP–GFP, we observed consistent localization of InR at the plasma membrane under each of these nutrient conditions, with a modest enhancement of the signal upon re-feeding (Fig. 6A–C,G). In contrast, starvation led to a significant decrease in InR membrane localization in Rab6-depleted cells, and its appearance in LAMP–GFP-marked puncta (Fig. 6D–G). Re-feeding failed to restore InR to the surface of Rab6-depleted cells. Clones of Rab6-null mutant cells displayed a similar pattern of InR localization, with a marked decrease at the plasma membrane and appearance of cytoplasmic puncta, which co-labeled with mCherry–Atg8a (Fig. S6A–C). Taken together, our results suggest that Rab6 regulates retrieval of InR from the endocytic pathway upon internalization to avoid its lysosomal degradation and ensure its recycling to the plasma membrane, thereby maintaining insulin signaling and inhibiting autophagy.

To address whether these effects of Rab6 are specific to InR localization or reflect a more general role in membrane protein trafficking, we examined the localization of two additional proteins: an mCherry-tagged version of the v-ATPase subunit VhaM8.9 (also known as ATP6AP2), which localizes to both plasma membrane and late endo/lysosomes, and a GFP-tagged human transferrin receptor, which cycles between the plasma membrane and recycling endosomes. In both cases, depletion of Rab6 led to a reduction in plasma membrane localization and an expansion of the punctate pool (Fig. S6D–G). Notably, the Rab5-positive early endosomes were also enlarged in Rab6 depleted cells, but remained distinct from the VhaM8.9-marked compartment (Fig. S6E), indicating that early and late endosomes retain their separate identities. The similar effects on InR, VhaM8.9 and hTfR suggest that Rab6 is a general regulator of plasma membrane bound protein recycling.

Rab6 has been shown to regulate several trafficking routes between the Golgi and plasma membrane, ER and endosomal membranes. In an effort to further characterize the mechanisms through which Rab6 regulates the sorting of cathepsins and plasma membrane-bound proteins, we depleted several Golgi-related and coat proteins. Knockdown of *Drosophila* orthologs of COG or GARP subunits did not phenocopy the effect of Rab6 depletion on accumulation of mCherry–Atg8a puncta or cell size (data not

Journal of Cell Science (2018) 131, jcs216127. doi:10.1242/jcs.216127

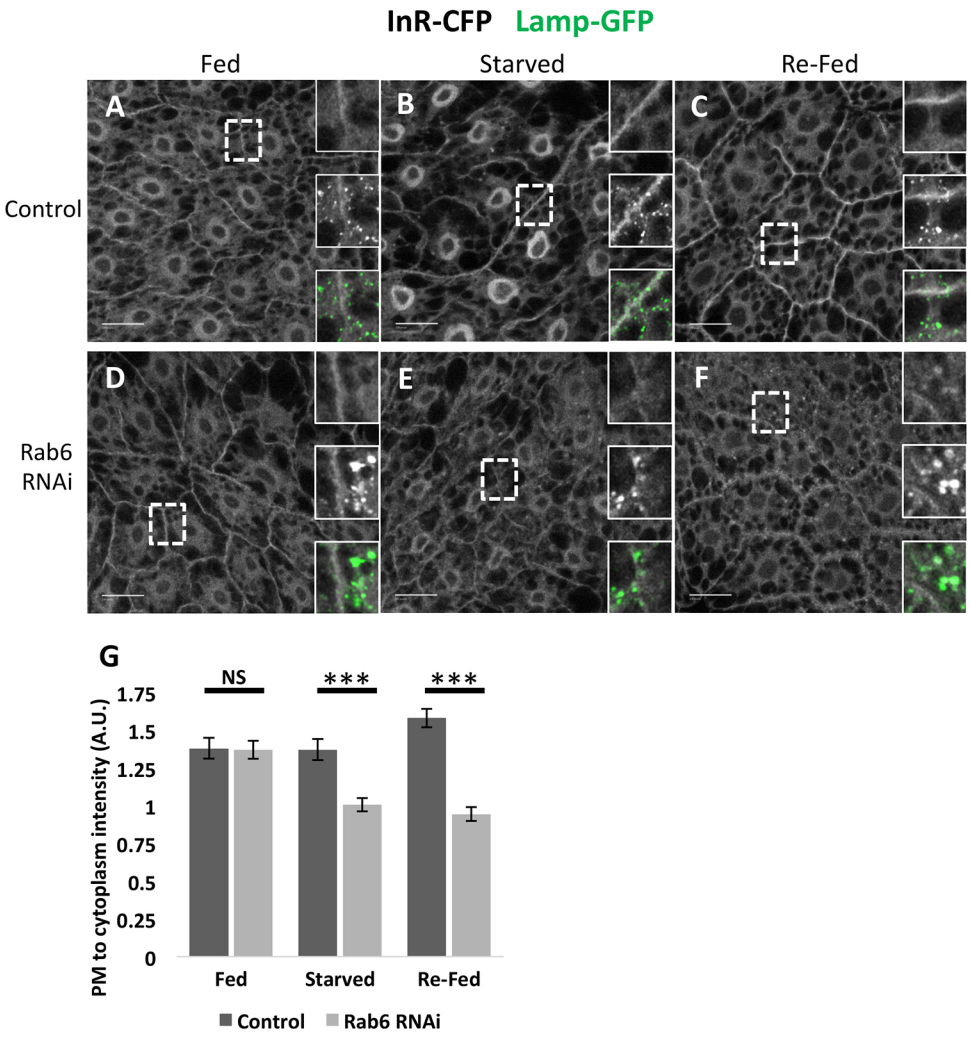

Fig. 6. Rab6 depletion results in mis-localization of the insulin receptor. Representative images of InR–CFP are shown in grayscale for control (A–C) and Rab6-depleted (D–F) fat body cells under fed, 4 h starved and 7 h re-fed conditions as indicated. Insets show an increased magnification of InR–CFP (top), LAMP–GFP (middle) and merge (bottom; LAMP-GFP in green). Quantified ratio of plasma membrane (PM) to cytoplasmic InR–CFP signal is shown in G. n=10 larvae and 20 cells analyzed per condition and genotype. ***P<0.01 (Student's t-test). Error bars indicate s.e.m. Scale bars: 25 µm. Genotypes: A–C, *Cg-Gal4, UAS-GFP-Lamp/+; UAS-InR-CFP/+*; D–F, *Cg-Gal4, UAS-GFP-Lamp/+; UAS-Rab6-dsRNA/ UAS-InR-CFP*.

shown). Similarly, depletion of the retromer subunit Vps35, or of the Golgi-associated proteins Arf1 or GRASP65 did not disrupt InR localization under fed or starvation conditions (Fig. S7A–I). These results suggest that the defective sorting of InR in Rab6 mutant cells is unlikely to result from a global defect in Golgi function. Collectively, our observations suggest that Rab6 is required to maintain homeostasis in the endomembrane system, autophagy and insulin signaling.

DISCUSSION

Rab6 is a classic trans-Golgi marker with established roles in the regulation of protein secretion and retrograde endosome-to-Golgi traffic (Goud et al., 1990; Luo and Gallwitz, 2003). However, a role in coordinating the reciprocal regulation between TOR signaling and autophagy during distinct nutrient states remains an unexplored topic. Here, we have characterized the role of Rab6 as a novel GTPase required to maintain a balance between autophagy and canonical insulin signaling in the larval fat body of flies.

Rab6 in yeast (Ypt6) has an established role in the sorting of vacuolar hydrolases, such as CPY and APE1, by regulating endosome-to-Golgi traffic (Luo and Gallwitz, 2003; Tsukada and Gallwitz, 1996). Ypt6 mediates the recruitment of the Golgi-associated retrograde protein (GARP) tethering complex to the Golgi to ensure retrieval of lysosomal sorting receptors such as Vps10 (Siniossoglou and Pelham, 2001). Loss of Ypt6 or its guanine exchange factor Ric1/Rgp1 also leads to defects in autophagy (Ohashi and Munro, 2010; Yang and Rosenwald, 2016; Ye et al., 2014). Interaction between Rab6 and GARP is conserved in mammalian cells, where depletion of GARP subunits blocks the delivery of lysosomal enzymes, leading to defective autophagy and swollen lysosomes, presumably due to an accumulation of non-degraded substrates (Liewen et al., 2005; Pérez-Victoria et al., 2008, 2010). Consistent with these findings, we observed expansion of the lysosomal compartment and reduced degradation of the autophagic substrate Ref(2)p when Rab6 was disrupted in fat body cells. Loss of Rab6 selectively prevented delivery of hydrolases, but not other lysosomal proteins, such as v-ATPase subunits or LAMP. Although these results are consistent with a role for Rab6 in the retrograde trafficking of a hydrolase receptor from the lysosome to the Golgi, localization of the *Drosophila* hydrolase receptor LERP was unaffected in Rab6 mutant cells. Interestingly, mutations in subunits of the retromer complex also disrupt lysosomal hydrolase delivery independently of LERP, leading to loss of autophagy and aberrant lysosomal structure (Maruzs et al., 2015). Altogether, these findings and similarities support a LERP-independent role for Rab6 in the regulation of hydrolase sorting in flies.

Recently, genetic screens in yeast identified three Rab genes, including the Rab6 ortholog *YPT6*, whose disruption leads to

Journal of Cell Science (2018) 131, jcs216127. doi:10.1242/jcs.216127

rapamycin sensitivity, a phenotype common to genes in the TOR pathway (Yang and Rosenwald, 2017). Depletion of *YPT6* did not block activation of TOR by amino acids, and its role in TOR signaling has not been defined. Similarly, it was previously found that depletion of a number of Rab proteins in *Drosophila* S2 cells, including Rab6, leads to modest decreases in TOR activity through unknown mechanisms (Li et al., 2010). In addition to its role in lysosomal enzyme delivery, our genetic data indicate that Rab6 acts specifically in the insulin signaling branch upstream of TOR: Rab6 was required for full activation of both Akt and S6K, and overexpression of Rheb or mutation of Pten rescued defects associated with Rab6 loss. Although the mis-sorting of InR in Rab6 mutant cells provides a potential explanation for these results, loss of Rab6 reduced cell size only modestly compared to $Inr^{-/-}$ or $Tor^{-/-}$ cells, and it affected the membrane localization of other proteins in addition to InR, suggesting that its contribution to TOR signaling is likely to be complex. Consistent with results in yeast, the failure of constitutively active RagA to rescue Rab6 mutant phenotypes suggests that Rab6 does not act in amino acid sensing upstream of TOR. Altogether, the genetic data presented here support a novel role for Rab6 in the insulin signaling pathway upstream of TOR.

The mechanisms responsible for trafficking of InR remain incompletely understood. Here, we show that loss of Rab6 results in a progressive internalization and misrouting of InR from its normal location at the plasma membrane to an accumulation in the lysosomal compartment. We observed similar effects on the location of other plasma membrane proteins including a v-ATPase subunit and the human transferrin receptor, suggesting that Rab6 may play a wider role in the trafficking of membrane-bound proteins. Indeed, Rab6 and its guanine nucleotide exchange factor RICH have been shown to regulate docking of internalized recycling endosomes with the trans-Golgi network before recycling towards the plasma membrane is completed (Iwanami et al., 2016; Miserey-Lenkei et al., 2007). In mammals, internalized glucose transporter 4 (GLU4) is sorted to the Golgi before being recycled to the plasma membrane in a nutrient-dependent manner (Brewer et al., 2014). Our data support a role for Rab6 in the regulation of a similar traffic route for InR. Components of the retromer complex also control delivery of plasma membrane proteins through a retrograde endosome to Golgi route and are synthetic lethal with Rab6/Yptg6 mutants in yeast, further suggesting that they regulate a common pathway (Klinger et al., 2015; Luo and Gallwitz, 2003). Here, we found that depletion of the retromer subunit Vps35 did not disrupt sorting of InR in fat body cells under fed or starvation conditions. Similarly, Inr localization was not affected by depletion of the Golgi regulators Grasp65 or Arf1. Our collective data therefore support a Rab6-specific sorting mechanism for membrane-bound proteins rather than defects of global Golgi function or coordinated traffic at the Golgi.

Accumulation of autophagic vesicles can result from an imbalance between their production and degradation, a phenomenon termed autophagic stress and first described in cathepsin D-deficient mice (Chu, 2006; Koike et al., 2000; Walls et al., 2007). Our data suggest that, similar to what is seen in animals deficient for cathepsin D, Rab6 mutant cells accumulate degradation-deficient autolysosomes as a result of their failure to deliver lysosomal enzymes (Fig. 7). This autophagic stress is further amplified by an overproduction of autophagosomes resulting from reduced insulin signaling due to internalization of InR. Together, these dual functions of Rab6 help to prevent autophagic stress by promoting a reciprocal balance between autophagic induction and capacity.

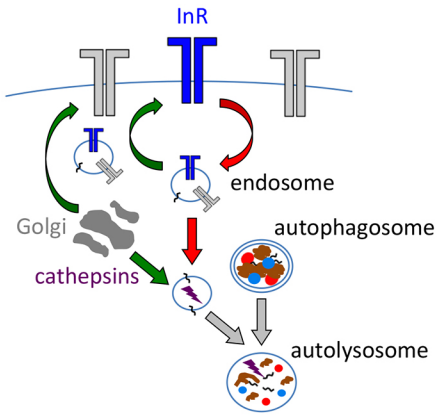

Fig. 7. Model of Rab6 function in InR trafficking and autophagy. Activities promoted and inhibited by Rab6 are indicated by green and red arrows, respectively. Rab6 maintains normal cell growth and autophagy inhibition by promoting the targeting and recycling of InR and other proteins to the plasma membrane, and supports lysosomal function through proper sorting of lysosomal hydrolases. In the absence of Rab6, membrane proteins are misrouted towards a defective endolysosomal pathway with deficient hydrolase activity, and reduced insulin signaling leads to induction of autophagy. By balancing the rate of autophagosome production with lysosomal capacity, Rab6 limits autophagic stress.

MATERIALS AND METHODS

Fly strains and genetic manipulations

Flies were raised at 25°C on standard cornmeal/molasses/agar medium. The following *D. melanogaster* strains were used: $Rab6^{D23D}$FRT40A (gift from Anne Ephrusi, European Molecular Biology Laboratory, Heidelberg, GE), UAS-RagA-Q61L (Kim et al., 2008), UAS-Rheb (gift from Bruce Edgar, University of Utah, UT), $Pten^{DJ189}$FRT40A (Gao et al., 2000), UAS-GFP-Ref(2)p and UAS-mCherry-Atg8a (Chang and Neufeld, 2009), UAS-Rab5-GFP (gift From David Bilder, University of Berkeley, CA, USA), UAS-mCherry-VhaM8.9, UAS-GFP-VhaM8.9 (gift from Matias Simmons, University of Freirburg, Freiburg, Germany), UAS-Vha55-EGFP (gift from Julian Dow, University of Glasgow, Glasgow, UK), UAS-LAMP-GFP and UAS-hrp-Lamp (gift from Helmut Krämer, University of Texas, Dallas, TX), UAS-InR-CFP (gift from Hugo Stocker, Institute of Molecular System Biology, Zurich, Switzerland) and Tubulin-Lerp-GFP (gift from Julie Brill, University of Toronto, Toronto, CA). The following additional strains were obtained from the Bloomington Stock Center (Bloomington, IN) or Vienna *Drosophila* RNAi Center (Vienna, Austria): *UAS-YFP.Rab6{CG10082[01]}*, Rab6 RNAi: *TRiP JF02640*, *UAS-Rheb{AV4}*, *UAS-Rab7.GFP{3}*, *UAS-hTfR.GFP{3}*, *UASp-RFP.Golgi{5}*, CathD RNAi: *GD5487,* CathL RNAi: *KK107765*, Vps35 RNAi: *TRiP HMS01858*, Arf1 RNAi: *TRiP JF01809*, and Grasp65 RNAi: *TRiP HMS01093*. *Cg-Gal4* (Hennig et al., 2006) and *r4-Gal4* (Bloomington, IN) were used for the expression of transgenes in a fat body-specific manner.

Heat shock-induced flippase (hsFLP)/flippase recognition target (FRT)-mediated loss of function clones in the larval fat body were induced in 0–4 h embryos by a 1–1.5 h heat shock at 37°C and were marked by fat body-specific activation of upstream activating sequence (UAS)-green fluorescent protein (GFP) lines on FRT-linked chromosomes. 'Flip-out' clones were generated through spontaneous hsFLP-dependent activation of Act>CD2>GAL4.

Autophagy induction and detection

To induce starvation, 25–30 larvae were transferred to fresh medium at 72 h after egg laying for 16–24 h to avoid crowded conditions. Afterwards they were transferred to 20% sucrose solution for 4 h before dissection. LysoTracker Red (Invitrogen) staining was performed as described previously (Juhasz and Neufeld, 2008).

Re-feeding experiments

A total of 25–30 larvae were transferred to fresh medium, 72 h after egg laying, for 16–24 h to avoid crowded conditions. Afterwards they were

transferred to 20% sucrose solution for 4 h before dissection followed by transfer of 10–15 larvae to regular laboratory cornmeal food mixed with 1 ml of water plus a fine granulated layer of yeast pellets covering the food for a duration of 6 h for western blot purposes or 7 h for imaging.

Immunohistochemistry

For imaging and analysis of fluorescently tagged proteins, 10–12 larvae per genotype were dissected and inverted in PBS and fixed overnight at 4°C in 4% paraformaldehyde in PBS. The next day, samples were washed extensively in PBS plus 0.1% Triton X-100 (PBST), and counterstained with DAPI. A single section or lobe of fat body from each carcass was dissected and mounted in VectaShield.

Samples to be used for immunohistochemistry were fixed and washed as above. Subsequently, they were blocked in PBST plus 4% normal goat serum for 3 h at room temperature and then incubated overnight in blocking solution containing the primary antibody of interest. The following antibodies and concentrations were used: cathepsin D (1:300; gift from André Dennes, Universitaets-Klinikum-Muenster, Muester, Germany), CP1/Cath L (1:250; gift from Patrick Dolph, Darthmouth College, NH), rabbit anti-GFP (1:30,000; catalog number A-11122, Molecular Probes) and anti-HRP (1:500, Jackson ImmunoResearch).

Confocal images were captured on a Zeiss LSM710 confocal microscope equipped with a 40× (W) objective lens (APO DIC III numerical aperture 1.2) and acquired using Zeiss software Zen 2010. Laser lines used in this study were 405, 488 and 561 nm. Red-green-blue (RGB) and grayscale images were further processed with ImageJ or Photoshop CS3. Live images of LysoTracker Red-stained samples were obtained on a Zeiss Axioscope-2 microscope equipped with a Nikon DXM1200 digital camera (Melville, NY), using a 40× Plan-Neofluar 0.75 NA objective lens and Nikon ACT-1 software. Images were further processed and assembled into figures using Adobe Photoshop CS (San Jose, CA) and ImageJ.

Statistical analysis and quantifications

Determination of puncta number, puncta size and cell size were performed using the 'analyze particle' command of ImageJ Software and the 'histogram' function of Adobe Photoshop CS3. Each clonal cell was traced along the cell membrane border to establish area to be used for quantification purposes in both programs. Neighboring wild-type cells, adjacent to experimental clonal cells, were used as internal controls for the experiments and statistical analysis. For non-clonal experiments, experimental and control samples were imaged under identical instrument settings and conditions to allow for comparisons between samples. *n* values for larvae, clone and cell number are indicated in the figure legends. Relative area occupied by autophagic vesicles was measured in pixels, at 3.8 pixels per micron.

For InR–CFP experiments, CFP signal was detected using a DAPI filter set. Measurements for statistical analysis were obtained using the box-plot function of ImageJ. The final signal values were obtained by averaging the highest signal peak in the plasma membrane subtracted from the highest peaks in the cytoplasm. Two cells per fat body were used for analysis from a total of 10 larvae. Statistical significance was evaluated by Student's *t*-test (Microsoft Excel).

Western blot analysis

Far bodies were dissected in PBS and lysed directly in SDS sample buffer. Extracts were boiled for 3 min, separated by polyacrylamide gel electrophoresis and transferred to Immobilon-P membranes (Millipore, Billerica MA). The following antibodies were used: rabbit anti-phospho-T398 dS6K (1:250; Cell Signaling Technology, Beverly, MA), rabbit anti-GFP (1:30,000; catalog number A-11122, Molecular Probes), mouse anti-β-tubulin E7 (1:250; Developmental Studies Hybridoma Bank, Iowa City, IA), rabbit anti-phospho-S505 Akt (1:1000; Cell Signaling Technology, Beverly, MA). Signals were visualized by using Super Signal West Pico chemiluminescent substrate (Thermo Scientific, Rockford, IL) with BioMax Light (Kodak, Rochester NY) or HyBlot CL autoradiography film (Denville Scientific, Metuchen NJ) and quantified using Adobe Photoshop software. Five larvae were used per sample condition and genotype. Each western blot experiment was performed as three independent biological replicates for all conditions and genotypes. Western blot films were exported to Adobe Photoshop CS3 and the images were inverted to black and white for band measurements. Student's *t*-test statistical analysis was used to compare all genotype and conditions tested using the mean from triplicate measurements.

Acknowledgements

We would like to thank Drs Anne Ephrusi, Bruce Edgar, David Bilder, Matias Simmons, Julian Dow, Helmut Krämer, Hugo Stocker, Julie Brill, André Dennes and Patrick Dolph for generous gifts of flies and antibodies. We also thank the Vienna Drosophila RNAi Center, the Bloomington Drosophila Stock Center and the Developmental Studies Hybridoma Bank at the University of Iowa for providing fly stocks and antibodies.

Competing interests

The authors declare no competing or financial interests.

Author contributions

Conceptualization: C.I.A., T.P.N.; Formal analysis: C.I.A., J.K.; Investigation: C.I.A., J.K.; Resources: T.N.; Writing - original draft: C.I.A.; Writing - review & editing: C.I.A., T.P.N.; Supervision: T.P.N.; Project administration: T.P.N.; Funding acquisition: T.P.N.

Funding

This work was supported by National Institutes of Health (grant R01 GM62509) to T.P.N. Deposited in PMC for release after 12 months.

Supplementary information

Supplementary information available online at
http://jcs.biologists.org/lookup/doi/10.1242/jcs.216127.supplemental

References

Ao, X., Zou, L. and Wu, Y. (2014). Regulation of autophagy by the Rab GTPase network. *Cell Death Differ.* **21**, 348-358.

Brewer, P. D., Habtemichael, E. N., Romenskaia, I., Mastick, C. C. and Coster, A. C. F. (2014). Insulin-regulated Glut4 translocation: membrane protein trafficking with six distinctive steps. *J. Biol. Chem.* **289**, 17280-17298.

Chang, Y.-Y. and Neufeld, T. P. (2009). An Atg1/Atg13 complex with multiple roles in TOR-mediated autophagy regulation. *Mol. Biol. Cell* **20**, 2004-2014.

Chen, Y. and Yu, L. (2017). Recent progress in autophagic lysosome reformation. *Traffic* **18**, 358-361.

Chu, C. T. (2006). Autophagic stress in neuronal injury and disease. *J. Neuropathol. Exp. Neurol.* **65**, 423-432.

Dennes, A., Cromme, C., Suresh, K., Kumar, N. S., Eble, J. A., Hahnenkamp, A. and Pohlmann, R. (2005). The novel Drosophila lysosomal enzyme receptor protein mediates lysosomal sorting in mammalian cells and binds mammalian and Drosophila GGA adaptors. *J. Biol. Chem.* **280**, 12849-12857.

Fader, C. M., Sánchez, D., Furlán, M. and Colombo, M. I. (2008). Induction of autophagy promotes fusion of multivesicular bodies with autophagic vacuoles in k562 cells. *Traffic* **9**, 230-250.

Foti, M., Moukil, M. A., Dudognon, P. and Carpentier, J. L. (2004). Insulin and IGF-1 receptor trafficking and signalling. *Novartis Found. Symp.* **262**, 125-141; discussion 141-7, 265-8.

Gao, X., Neufeld, T. P. and Pan, D. (2000). Drosophila PTEN regulates cell growth and proliferation through PI3K-dependent and -independent pathways. *Dev. Biol.* **221**, 404-418.

Goberdhan, D. C. I., Paricio, N., Goodman, E. C., Mlodzik, M. and Wilson, C. (1999). Drosophila tumor suppressor PTEN controls cell size and number by antagonizing the Chico/PI3-kinase signaling pathway. *Genes Dev.* **13**, 3244-3258.

Goh, L. K. and Sorkin, A. (2013). Endocytosis of receptor tyrosine kinases. *Cold Spring Harb. Perspect. Biol.* **5**, a017459.

Goud, B., Zahraoui, A., Tavitian, A. and Saraste, J. (1990). Small GTP-binding protein associated with Golgi cisternae. *Nature* **345**, 553-556.

Gutierrez, M. G., Munafo, D. B., Beron, W. and Colombo, M. I. (2004). Rab7 is required for the normal progression of the autophagic pathway in mammalian cells. *J. Cell Sci.* **117**, 2687-2697.

Hennig, K. M., Colombani, J. and Neufeld, T. P. (2006). TOR coordinates bulk and targeted endocytosis in the Drosophila melanogaster fat body to regulate cell growth. *J. Cell Biol.* **173**, 963-974.

Hirota, Y. and Tanaka, Y. (2009). A small GTPase, human Rab32, is required for the formation of autophagic vacuoles under basal conditions. *Cell. Mol. Life Sci.* **66**, 2913-2932.

Hutagalung, A. H. and Novick, P. J. (2011). Role of Rab GTPases in membrane traffic and cell physiology. *Physiol. Rev.* **91**, 119-149.

Iwanami, N., Nakamura, Y., Satoh, T., Liu, Z. and Satoh, A. K. (2016). Rab6 is required for multiple apical transport pathways but not the basolateral transport pathway in Drosophila photoreceptors. *PLoS Genet.* **12**, e1005828.

Jager, S., Bucci, C., Tanida, I., Ueno, T., Kominami, E., Saftig, P. and Eskelinen, E. L. (2004). Role for Rab7 in maturation of late autophagic vacuoles. *J. Cell Sci.* **117**, 4837-4848.
Jiang, P. and Mizushima, N. (2014). Autophagy and human diseases. *Cell Res.* **24**, 69-79.
Juhasz, G. and Neufeld, T. P. (2008). Experimental control and characterization of autophagy in Drosophila. *Methods Mol. Biol.* **445**, 125-133.
Kim, E., Goraksha-Hicks, P., Li, L., Neufeld, T. P. and Guan, K.-L. (2008). Regulation of TORC1 by Rag GTPases in nutrient response. *Nat. Cell Biol.* **10**, 935-945.
Klinger, S. C., Siupka, P. and Nielsen, M. S. (2015). Retromer-mediated trafficking of transmembrane receptors and transporters. *Membranes* **5**, 288-306.
Koike, M., Nakanishi, H., Saftig, P., Ezaki, J., Isahara, K., Ohsawa, Y., Schulz-Schaeffer, W., Watanabe, T., Waguri, S., Kametaka, S. et al. (2000). Cathepsin D deficiency induces lysosomal storage with ceroid lipofuscin in mouse CNS neurons. *J. Neurosci.* **20**, 6898-6906.
Li, L., Kim, E., Yuan, H., Inoki, K., Goraksha-Hicks, P., Schiesher, R. L., Neufeld, T. P. and Guan, K.-L. (2010). Regulation of mTORC1 by the Rab and Arf GTPases. *J. Biol. Chem.* **285**, 19705-19709.
Liewen, H., Meinhold-Heerlein, I., Oliveira, V., Schwarzenbacher, R., Luo, G., Wadle, A., Jung, M., Pfreundschuh, M. and Stenner-Liewen, F. (2005). Characterization of the human GARP (Golgi associated retrograde protein) complex. *Exp. Cell Res.* **306**, 24-34.
Lippai, M. and Szatmári, Z. (2017). Autophagy-from molecular mechanisms to clinical relevance. *Cell Biol. Toxicol.* **33**, 145-168.
Longatti, A., Lamb, C. A., Razi, M., Yoshimura, S., Barr, F. A. and Tooze, S. A. (2012). TBC1D14 regulates autophagosome formation via Rab11- and ULK1-positive recycling endosomes. *J. Cell Biol.* **197**, 659-675.
Luo, Z. and Gallwitz, D. (2003). Biochemical and genetic evidence for the involvement of yeast Ypt6-GTPase in protein retrieval to different Golgi compartments. *J. Biol. Chem.* **278**, 791-799.
Martinez, O., Schmidt, A., Salamero, J., Hoflack, B., Roa, M. and Goud, B. (1994). The small GTP-binding protein rab6 functions in intra-Golgi transport. *J. Cell Biol.* **127**, 1575-1588.
Maruzs, T., Lőrincz, P., Szatmári, Z., Széplaki, S., Sándor, Z., Lakatos, Z., Puska, G., Juhász, G. and Sass, M. (2015). Retromer ensures the degradation of autophagic cargo by maintaining lysosome function in Drosophila. *Traffic* **16**, 1088-1107.
Mauvezin, C., Ayala, C., Braden, C. R., Kim, J. and Neufeld, T. P. (2014). Assays to monitor autophagy in Drosophila. *Methods* **68**, 134-139.
Mauvezin, C., Nagy, P., Juhász, G. and Neufeld, T. P. (2015). Autophagosome-lysosome fusion is independent of V-ATPase-mediated acidification. *Nat. Commun.* **6**, 7007.
Mauvezin, C., Neisch, A. L., Ayala, C. I., Kim, J., Beltrame, A., Braden, C. R., Gardner, M. K., Hays, T. S. and Neufeld, T. P. (2016). Coordination of autophagosome-lysosome fusion and transport by a Klp98A-Rab14 complex in Drosophila. *J. Cell Sci.* **129**, 971-982.
Medigeshi, G. R. and Schu, P. (2003). Characterization of the in vitro retrograde transport of MPR46. *Traffic* **4**, 802-811.
Miserey-Lenkei, S., Couëdel-Courteille, A., Del Nery, E., Bardin, S., Piel, M., Racine, V., Sibarita, J.-B., Perez, F., Bornens, M. and Goud, B. (2006). A role for the Rab6A′ GTPase in the inactivation of the Mad2-spindle checkpoint. *EMBO J.* **25**, 278-289.
Miserey-Lenkei, S., Waharte, F., Boulet, A., Cuif, M.-H., Tenza, D., El Marjou, A., Raposo, G., Salamero, J., Héliot, L., Goud, B. et al. (2007). Rab6-interacting protein 1 links Rab6 and Rab11 function. *Traffic* **8**, 1385-1403.
Ohashi, Y. and Munro, S. (2010). Membrane delivery to the yeast autophagosome from the Golgi-endosomal system. *Mol. Biol. Cell* **21**, 3998-4008.
Pérez-Victoria, F. J., Mardones, G. A. and Bonifacino, J. S. (2008). Requirement of the human GARP complex for mannose 6-phosphate-receptor-dependent sorting of cathepsin D to lysosomes. *Mol. Biol. Cell* **19**, 2350-2362.
Pérez-Victoria, F. J., Schindler, C., Magadán, J. G., Mardones, G. A., Delevoye, C., Romao, M., Raposo, G. and Bonifacino, J. S. (2010). Ang2/fat-free is a conserved subunit of the Golgi-associated retrograde protein complex. *Mol. Biol. Cell* **21**, 3386-3395.
Purcell, K. and Artavanis-Tsakonas, S. (1999). The developmental role of warthog, the notch modifier encoding Drab6. *J. Cell Biol.* **146**, 731-740.
Ravikumar, B., Imarisio, S., Sarkar, S., O'Kane, C. J. and Rubinsztein, D. C. (2008). Rab5 modulates aggregation and toxicity of mutant huntingtin through macroautophagy in cell and fly models of Huntington disease. *J. Cell Sci.* **121**, 1649-1660.
Sancak, Y., Peterson, T. R., Shaul, Y. D., Lindquist, R. A., Thoreen, C. C., Bar-Peled, L. and Sabatini, D. M. (2008). The Rag GTPases bind raptor and mediate amino acid signaling to mTORC1. *Science* **320**, 1496-1501.
Scanga, S. E., Ruel, L., Binari, R. C., Snow, B., Stambolic, V., Bouchard, D., Peters, M., Calvieri, B., Mak, T. W., Woodgett, J. R. et al. (2001). The conserved PI3′K/PTEN/Akt signaling pathway regulates both cell size and survival in Drosophila. *Oncogene* **19**, 3971-3977.
Shimobayashi, M. and Hall, M. N. (2014). Making new contacts: the mTOR network in metabolism and signalling crosstalk. *Nat. Rev. Mol. Cell Biol.* **15**, 155-162.
Siniossoglou, S. and Pelham, H. R. (2001). An effector of Ypt6p binds the SNARE Tlg1p and mediates selective fusion of vesicles with late Golgi membranes. *EMBO J.* **20**, 5991-5998.
Stenmark, H. (2009). Rab GTPases as coordinators of vesicle traffic. *Nat. Rev. Mol. Cell Biol.* **10**, 513-525.
Tsukada, M. and Gallwitz, D. (1996). Isolation and characterization of SYS genes from yeast, multicopy suppressors of the functional loss of the transport GTPase Ypt6p. *J. Cell Sci.* **109**, 2471-2481.
Walls, K. C., Klocke, B. J., Saftig, P., Shibata, M., Uchiyama, Y., Roth, K. A. and Shacka, J. J. (2007). Altered regulation of phosphatidylinositol 3-kinase signaling in cathepsin D-deficient brain. *Autophagy* **3**, 222-229.
White, J., Johannes, L., Mallard, F., Girod, A., Grill, S., Reinsch, S., Keller, P., Tzschaschel, B., Echard, A., Goud, B. et al. (1999). Rab6 coordinates a novel Golgi to ER retrograde transport pathway in live cells. *J. Cell Biol.* **147**, 743-760.
Worby, C. A. and Dixon, J. E. (2014). Pten. *Annu. Rev. Biochem.* **83**, 641-669.
Yang, S. and Rosenwald, A. G. (2016). Autophagy in Saccharomyces cerevisiae requires the monomeric GTP-binding proteins, Arl1 and Ypt6. *Autophagy* **12**, 1721-1737.
Yang, S. and Rosenwald, A. (2017). A high copy suppressor screen for autophagy defects in saccharomyces arl1Delta and ypt6Delta strains. *G3* **7**, 333-341.
Ye, M., Chen, Y., Zou, S., Yu, S. and Liang, Y. (2014). Ypt1 suppresses defects of vesicle trafficking and autophagy in Ypt6 related mutants. *Cell Biol. Int.* **38**, 663-674.
Yu, L., McPhee, C. K., Zheng, L., Mardones, G. A., Rong, Y., Peng, J., Mi, N., Zhao, Y., Liu, Z., Wan, F. et al. (2011). Termination of autophagy and reformation of lysosomes regulated by mTOR. *Nature* **465**, 942-946.
Zhang, J., Schulze, K. L., Hiesinger, P. R., Suyama, K., Wang, S., Fish, M., Acar, M., Hoskins, R. A., Bellen, H. J. and Scott, M. P. (2007). Thirty-one flavors of Drosophila rab proteins. *Genetics* **176**, 1307-1322.
Zoppino, F. C. M., Militello, R. D., Slavin, I., Álvarez, C. and Colombo, M. I. (2010). Autophagosome formation depends on the small GTPase Rab1 and functional ER exit sites. *Traffic* **11**, 1246-1261.

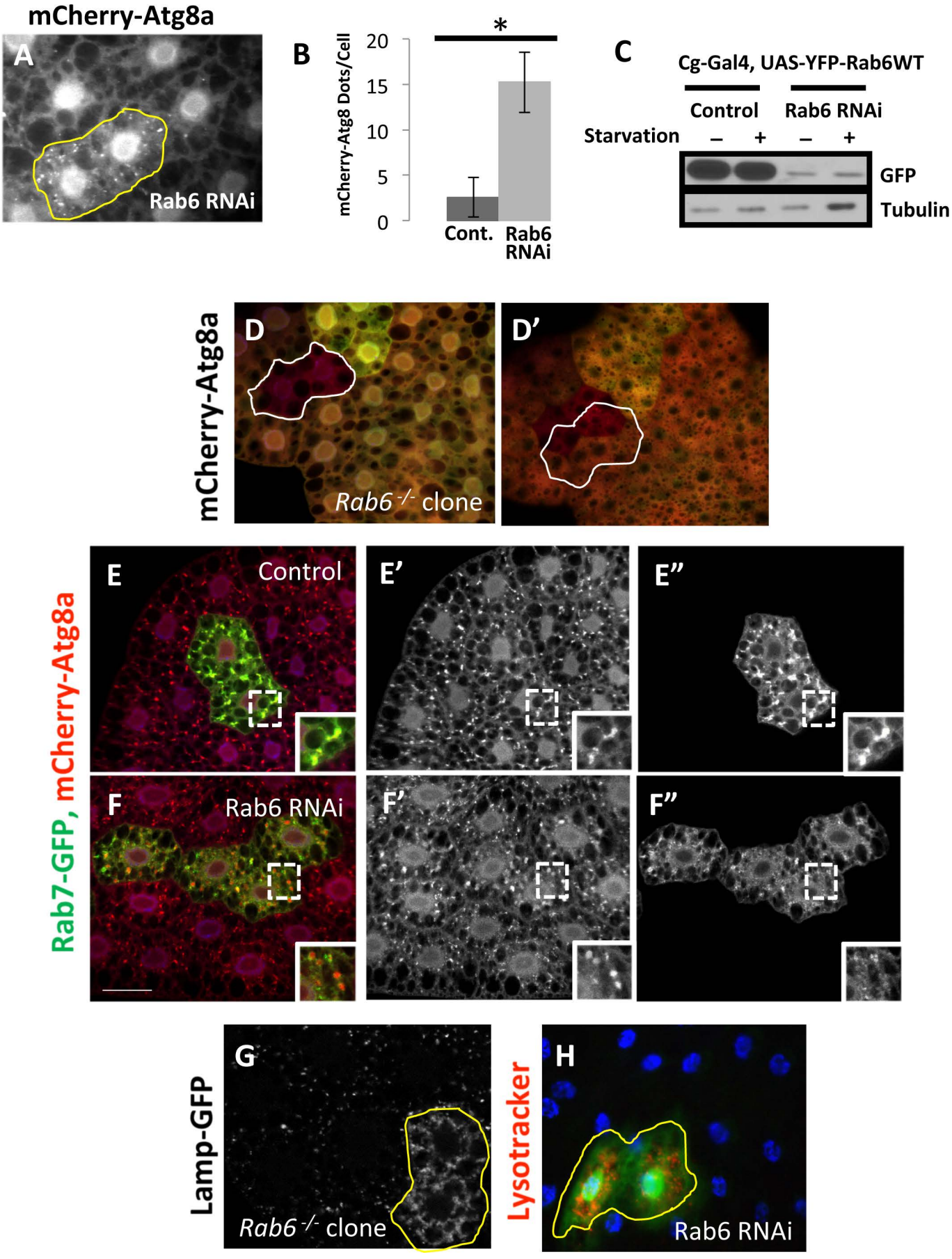
mCherry-Atg8a
A
Rab6 RNAi
B
mCherry-Atg8 Dots/Cell
20
15
10
5
0
*
Cont.
Rab6 RNAi
C
Cg-Gal4, UAS-YFP-Rab6WT
Control
Rab6 RNAi
Starvation
– + – +
GFP
Tubulin
mCherry-Atg8a
D
Rab6 -/- clone
D'
Rab7-GFP, mCherry-Atg8a
E
Control
E'
E''
F
Rab6 RNAi
F'
F''
Lamp-GFP
G
Rab6 -/- clone
Lysotracker
H
Rab6 RNAi

Figure S1. Loss of Rab6 leads to expansion of the lysosomal compartment and accumulation of autolysosomes.

A) Representative image of larval fat body containing a *Rab6* RNAi expressing cell clone (outlined in yellow), showing increased accumulation of mCherry-Atg8a-marked autophagic vesicles relative to surrounding control cells under fed conditions.

B) Mean number of mCherry-Atg8a punctate per cell in control (yw) and Rab6-depleted fat bodies is indicated. n=20 clones and 10 larvae analyzed per genotype. *p<0.05, Student's t-test. Error bars indicate standard error of the mean (s.e.m.).

C) YFP-Rab6 is reduced in extracts of Rab6-depleted fat body tissue under basal and starved conditions as compared to control fat body tissue. YFP-Rab6 was detected via western blot using a GFP antibody.

D) Representative images of larval fat body containing a *Rab6* null cell clone (outlined in white), showing absence of mCherry-Atg8a-marked autophagic vesicles similar to surrounding control cells under fed conditions in early L3 instar larvae. Nuclear (D) and cortical (D') focal planes are shown.

E,F) Representative image of larval fat body containing a control (E) or *Rab6* RNAi expressing (F) cell clone marked by expression of Rab7-GFP, under starvation conditions. mCherry-Atg8a-marked autophagic vesicles co-localize with Rab7-GFP under both conditions. E'-F') and E"-F") depict red and green channels, respectively for better visualization.

G) Representative image of larval fat body containing a *Rab6* null cell clone (outlined in yellow), showing expansion of Lamp-GFP labeled lysosomes relative to surrounding control cells under fed conditions.

H) Representative image of larval fat body containing a *Rab6* RNAi expressing cell clone (marked by GFP), showing increased accumulation of Lysotracker Red autolysosomes relative to surrounding control cells under fed conditions.

Scale bar, 25μm. Genotypes: A) *hs-flp; UAS-Dicer/+; r4-mCherry-Atg8a, Act<CD2<Gal4, UAS-GFP /UAS-Rab6-dsRNA.* C) *Control: Cg-Gal4, UAS-Rab6-WT-YFP/+; +/+. Rab6 RNAi: Cg-Gal4, UAS-Rab6-WT-YFP/+; UAS_Rab6-dsRNA/+.* D) *hs-flp; Rab6^{D23D}, FRT40A /UAS-2x-eGFP, FRT40A, fb-Gal4; UAS-mCherry-Atg8a/+.* E) *hs-flp; UAS-Rab7-GFP/+; r4-mCherry-Atg8a, Act<CD2<Gal4, /+.* F) *hs-flp; UAS-Rab7-GFP/+; r4-mCherry-Atg8a, Act<CD2<Gal4, /+.* G) *hs-flp; Rab6^{D23D}, FRT40A /UAS-ds-Red, FRT40A, fb-Gal4, UAS-Lamp-GFP; +/+.* H) *hs-flp; +/+; Act<CD2<Gal4, UAS-GFP/UAS-Rab6-dsRNA*

Journal of Cell Science • Supplementary information

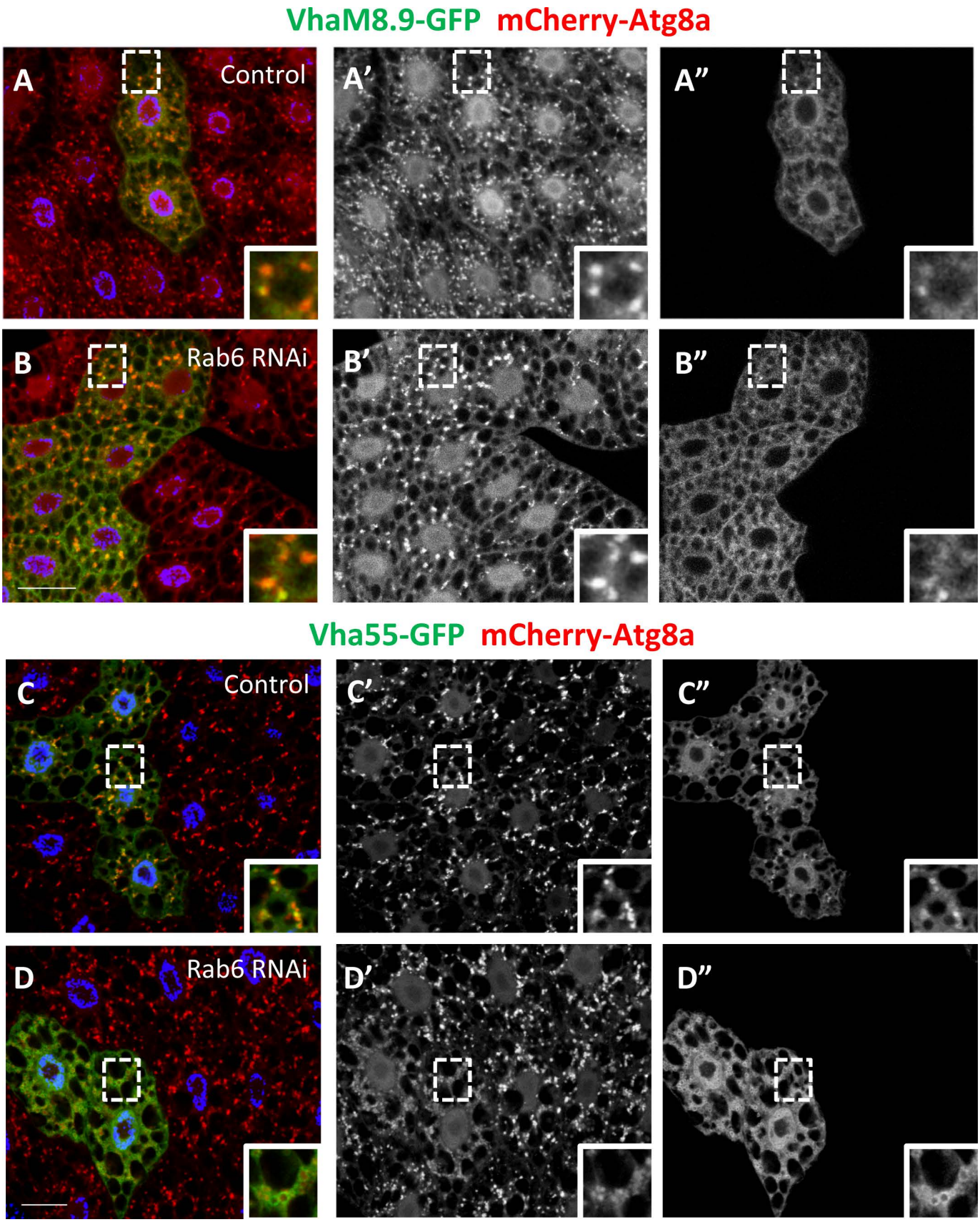

Journal of Cell Science • Supplementary information

Figure S2. Rab6 is not required for the recruitment of vacuolar ATPases to autophagic vesicles.

Representative images of larval fat body containing a control (A,C) or *Rab6* RNAi expressing (B,D) cell clone marked by expression of Vha8.9-GFP (A,B) or Vha55-GFP (C,D), under starvation conditions. mCherry-Atg8a-marked autophagic vesicles co-localize with v-ATPase subunits in both control and Rab6 depleted cells. mCherry (‘) and GFP (“) channels are shown separately in grayscale.

Scale bar, 25µm. Genotypes: A) *hs-flp; UAS-VhaM8.9-GFP/+; r4-mCherry-Atg8a, Act<CD2<Gal4, /+.* B) *hs-flp; UAS-VhaM8.9-GFP/+; r4-mCherry-Atg8a, Act<CD2<Gal4/UAS-Rab6-dsRNA.* C) *hs-flp; UAS-Vha55-GFP/+; r4-mCherry-Atg8a, Act<CD2<Gal4/+.* D) *hs-flp; UAS-Vha55-GFP/+; r4-mCherry-Atg8a, Act<CD2<Gal4/UAS-Rab6-dsRNA*

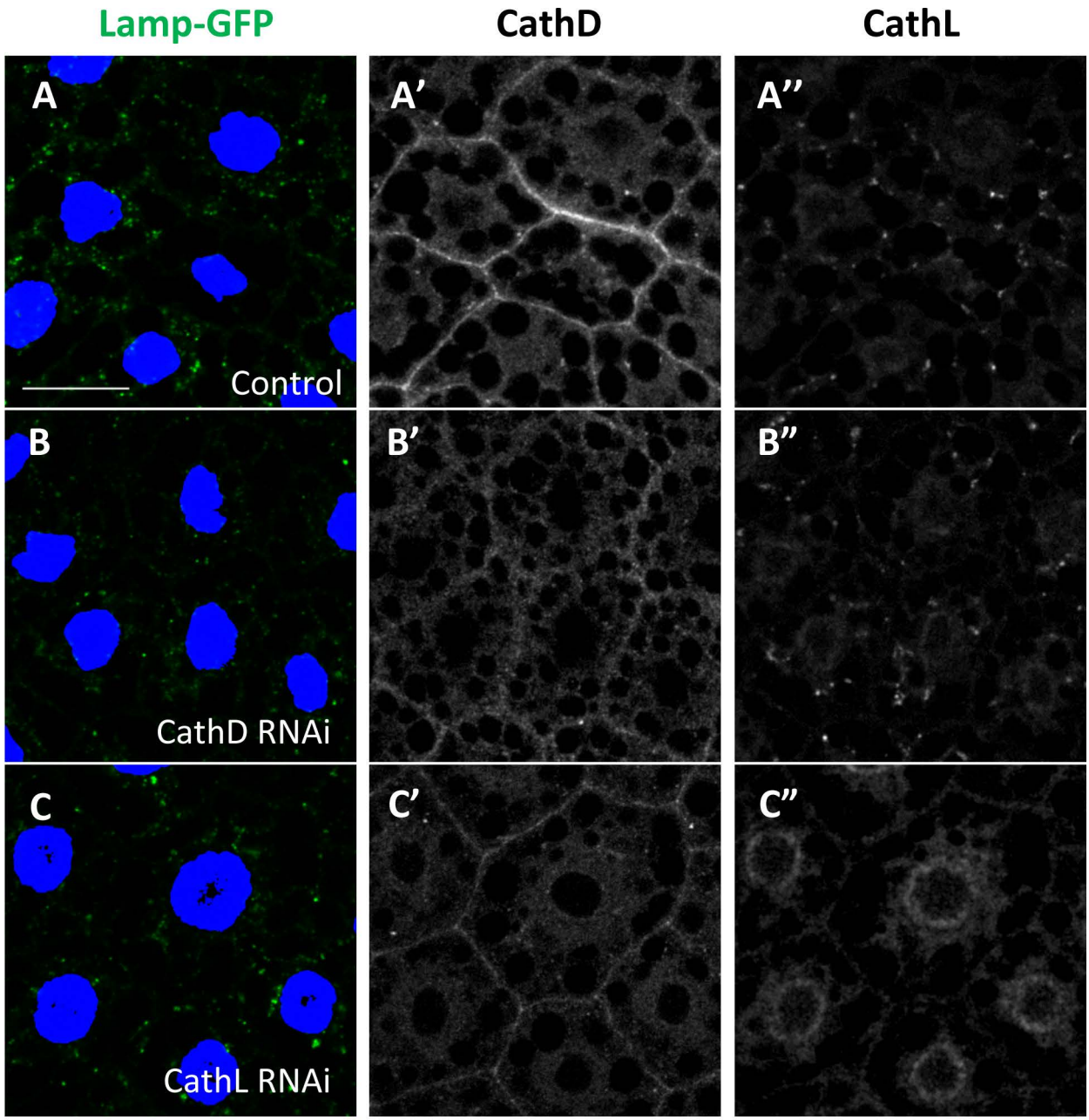

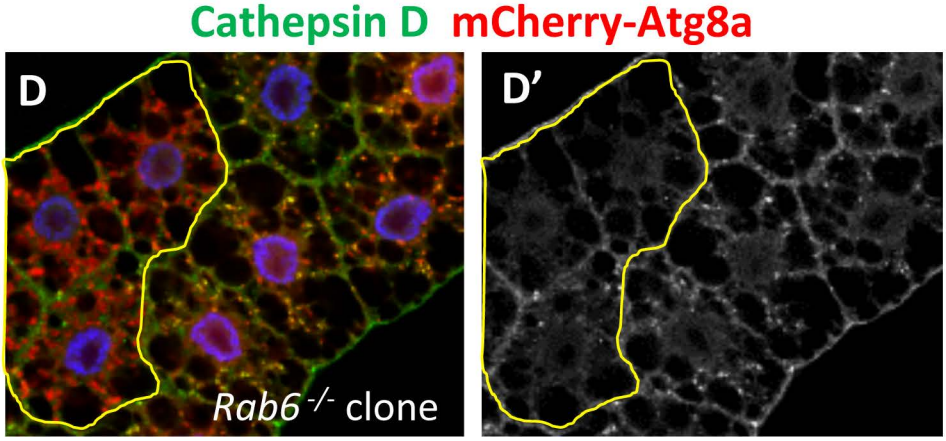

Figure S3. Cathepsin D and Cathepsin L localize to autolysosomes dependent on Rab6.

A-C) RNAi-mediated depletion of Cathepsin D (B) and Cathepsin L (C) throughout the larval fat body results in reduction of Cathepsin D (B') and Cathepsin L (C") staining from punctae that co-localize with the lysosomal compartment marker Lamp-GFP. Nuclei are marked by DAPI (blue).

D) Autolysosomal Cathepsin D staining (green) is reduced in Rab6 null cell clones (outlined in yellow). Cathepsin D staining is depicted in grayscale in (D'). 4hr starvation conditions.

Scale bar, 25μm. Genotypes: A) *Cg-Gal4 UAS-Lamp-GFP/+*. B) *Cg-Gal4 UAS-Lamp-GFP/UAS-CathD-dsRNA*. C) *Cg-Gal4 UAS-Lamp-GFP/UAS-CathL-dsRNA*. D) *hs-flp; Rab6^{D23D}, FRT40A /UAS-2x-eGFP, FRT40A, fb-Gal4; UAS-mCherry-Atg8a/+*.

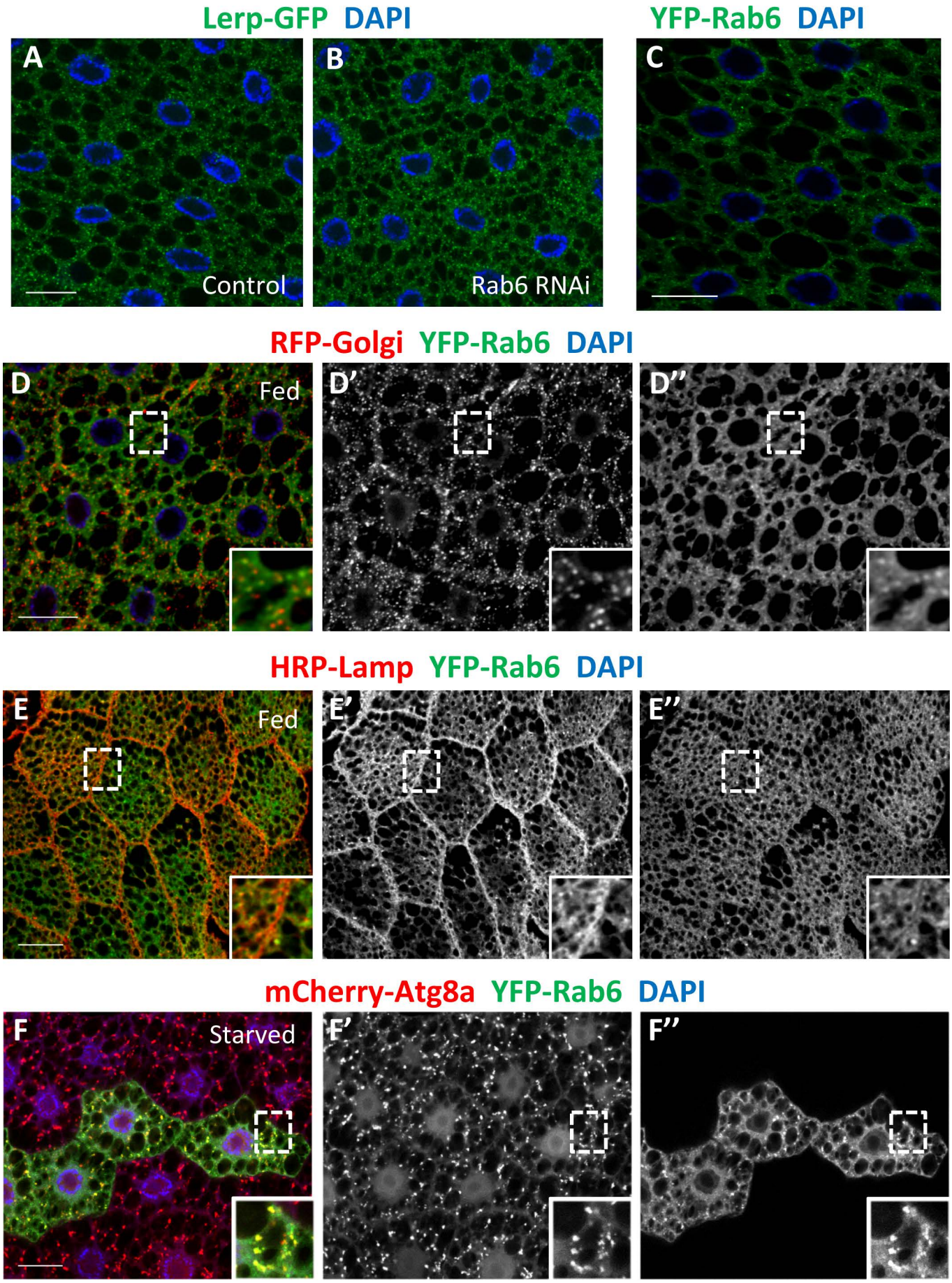

Journal of Cell Science • Supplementary information

Figure S4. Rab6 localizes to distinct subcellular compartments and is not required for LERP localization in fat body cells.

A,B) Lerp-GFP displays a similar punctate localization in control (A) and Rab6-depleted (B) fat body cells; fed conditions.

C) Representative image of larval fat body showing cytoplasmic distribution of YFP-Rab 6 under fed conditions.

D) Co-localization of YFP-Rab6 and RFP-Golgi expressed throughout the larval fat body under fed conditions. D',D") depict red and green channels, respectively, for better visualization.

E) Co-localization of YFP-Rab6 and HRP-Lamp expressed throughout the larval fat body under fed conditions. HRP antigen was visualized by immunostaining. E', E") depict red and green channels, respectively, for better visualization.

F) Representative image of larval fat body containing a cell clone marked by expression of YFP-Rab6, showing formation of punctae under starvation conditions that colocalize with mCherry-Atg8a-marked autophagic vesicles under 4hr starvation conditions. F', F") depict red and green channels, respectively, for better visualization.

Scale bar, 25μm. Genotypes: A,B) *control*: *Cg-Gal4/Tubulin-Lerp-GFP. Rab6 RNAi: Cg-Gal4/Tubulin-Lerp-GFP; UAS-Rab6-dsRNA/+.* C) *Cg-Gal4 UAS-YFP-Rab6.* D) *Cg-Gal4 UAS-YFP-Rab6/UAS-RFP-Golgi.* E) *Cg-Gal4 UAS-YFP-Rab6/UAS-HRP-Lamp.* F) *hs-flp; UAS-YFP-Rab6/+; r4-mCherry-Atg8a, Act<CD2<Gal4, /+.*

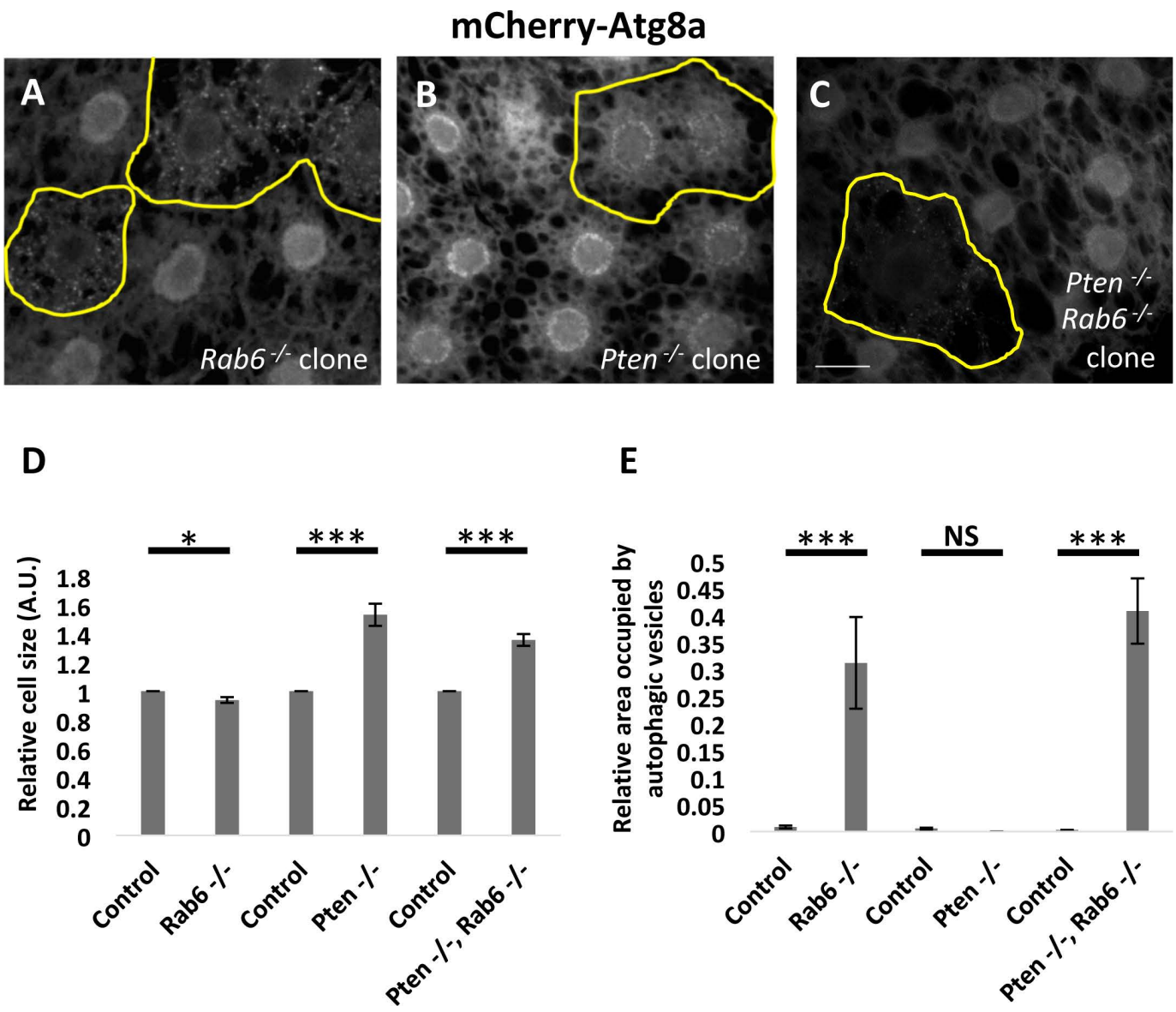

Figure S5. Cell size reduction in Rab6 null clones is rescued by deficiency of Pten.

A-C) Evaluation of mCherry-Atg8a marked autophagic vesicles under fed conditions in surrounding control cells and in *Rab6*$^{-/-}$ (A), *Pten*$^{-/-}$ (B), and *Rab6*$^{-/-}$ *Pten*$^{-/-}$ mutant clones (C).

D,E) Relative cell size and percent area occupied by mCherry-Atg8a punctae (each normalized to surrounding control cells) are indicated for the genotypes shown in in A-C.

Scalebar, 25 µm. Genotypes: A) *hs-flp; Rab6*^{D23D}*, FRT40A /UAS-2x-eGFP, FRT40A, fb-Gal4; UAS-mCherry-Atg8a/+.* B) *hs-flp; Pten*^{Dj189}*, FRT40A /UAS-2x-eGFP, FRT40A, fb-Gal4; UAS-mCherry-Atg8a/+.* C) *hs-flp; Rab6*^{D23D} *Pten*^{Dj189}*, FRT40A /UAS-2x-eGFP, FRT40A, fb-Gal4; UAS-mCherry-Atg8a/+.* N=10 larvae and 60 (A), 21 (B), 89 (C) clones analyzed per genotype. *p<0.05, ***p<0.01, NS p>0.05; Student's t-test. Error bars indicate s.e.m.

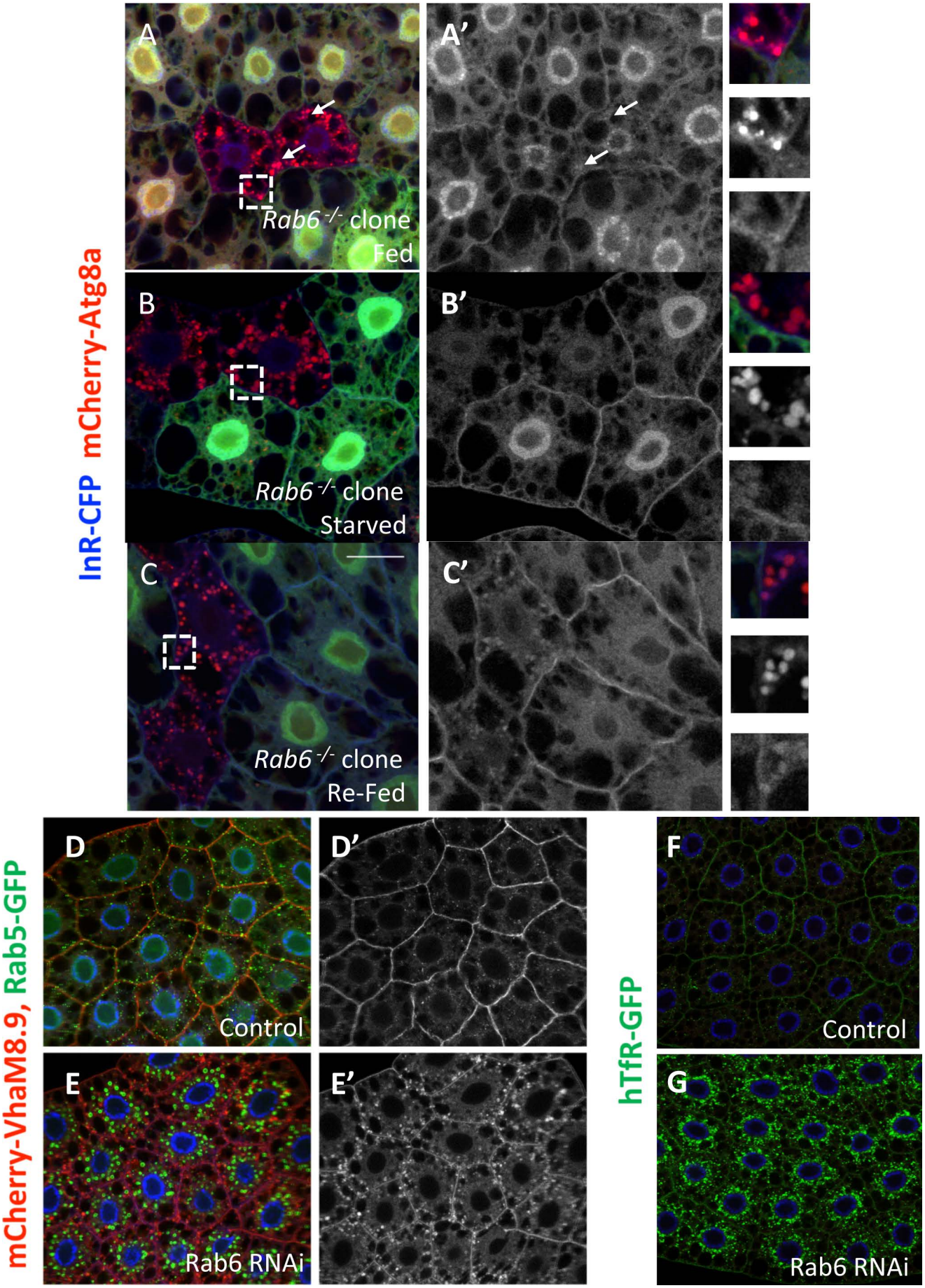
InR-CFP mCherry-Atg8a
A
A'
Rab6 -/- clone
Fed
B
B'
Rab6 -/- clone
Starved
C
C'
Rab6 -/- clone
Re-Fed
mCherry-VhaM8.9, Rab5-GFP
D
D'
Control
E
E'
Rab6 RNAi
hTfR-GFP
F
Control
G
Rab6 RNAi

Figure S6. Loss of Rab6 results in internalization of the insulin receptor independent of nutrient status and mis-localization of plasma membrane proteins.

A-C) Evaluation of mCherry-Atg8a marked autophagic vesicles and InR-CFP under basal states, starvation and full nutrient re-feeding in surrounding control cells and in *Rab6*$^{-/-}$ clones (marked by the absence of GFP). Blue channel (InR-CFP) for the distinct nutrient conditions is shown in grayscale in A', B' and C'. Insets show increased magnification of merge (top; Atg8a in red and InR-CFP in blue), mCherry-Atg8a (middle) and InR-CFP (bottom).

D-E) Depletion of Rab6 throughout the larval fat body results in expansion of the Rab5-GFP-marked early endosomal and VhaM8.9-mCherry late endosomal compartments (E) compared to control tissue (D); loss of plasma membrane localization of VhaM8.9 is also seen in Rab6 depleted tissue (E). D',E') depict red channel (mCherry-VhaM8.9) for better visualization. Fed conditions.

F-G) Depletion of Rab6 throughout the larval fat body results in expansion of the human Transferrin Receptor (hTfR)-GFP-marked recycling endosomal compartment (G) compared to control tissue (F). Fed conditions.

Scalebar, 25 µm. Genotypes: A-C) *hs-flp; Rab6*^{D23D}*, FRT40A /UAS-2x-eGFP, FRT40A, fb-Gal4; UAS-mCherry-Atg8a/UAS-InR-CFP.* D) *Cg-Gal4, UAS-mCherry-VhaM8.9/+; UAS-Rab5-GFP/+. E) Cg-Gal4, UAS-mCherry-VhaM8.9/+; UAS-Rab5-GFP/UAS-Rab6-dsRNA F) Cg-Gal4/+; UAS-hTfR-GFP/+. G) Cg-Gal4/+; UAS-hTfR-GFP/UAS-Rab6-dsRNA*

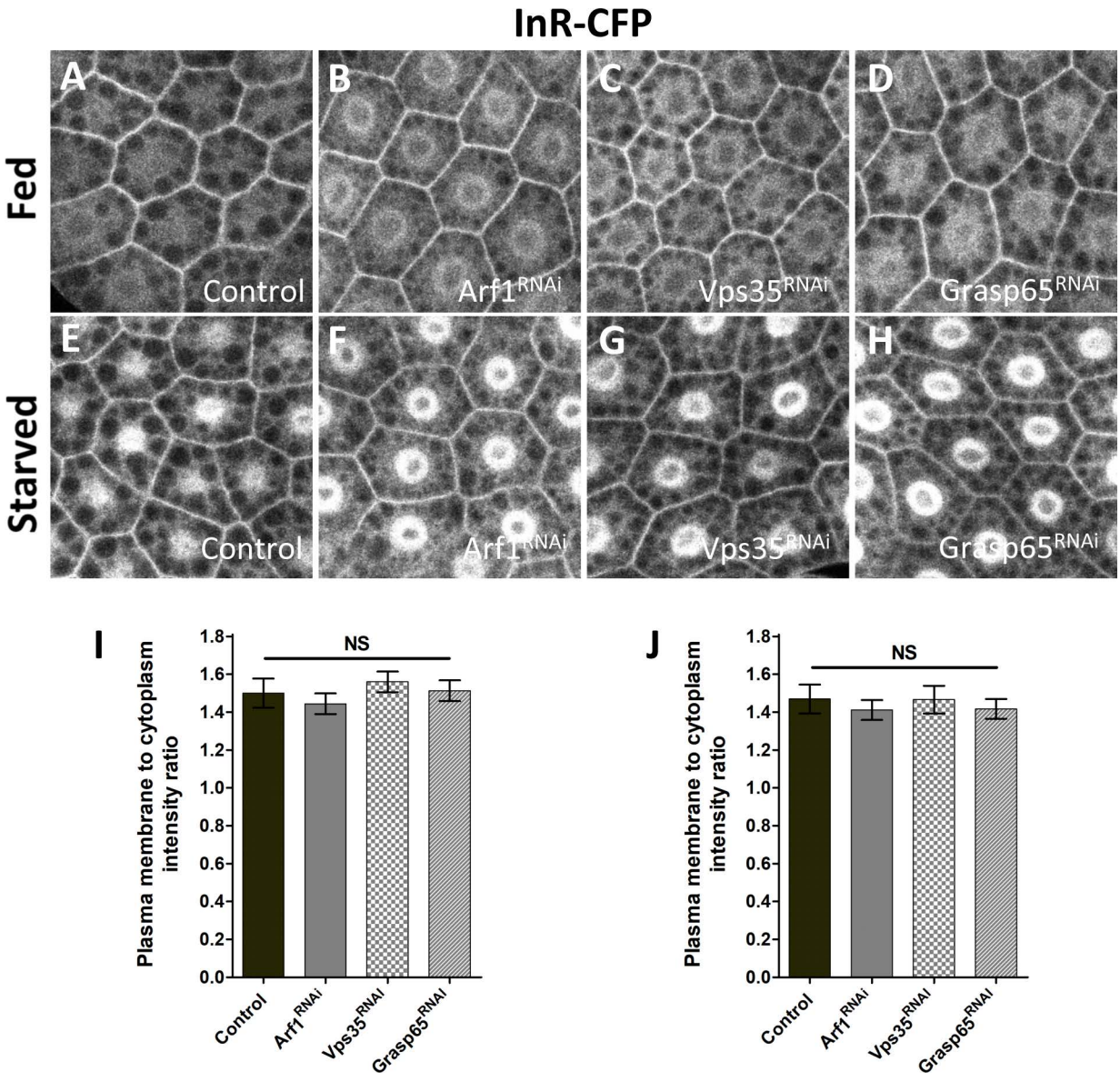

Figure S7. Effect of Golgi-associated protein depletion on InR localization.

Representative images of InR-CFP are shown in grayscale for control (A, E), Arf1- (B, F), Vps35- (C, G) and GRASP-65-depleted (D, H) fat body cells under fed and 4-hr starvation conditions as indicated. Quantified ratio of plasma membrane to cytoplasmic InR-CFP signal is shown in I (fed) and J (starved). n=10 larvae and 20 cells analyzed per condition and genotype. NS, p>0.05; Student's t-test. Error bars indicate s.e.m.

Genotypes: A, E) *Cg-Gal4/+; UAS-InR-CFP/+*. B, F) *Cg-Gal4/+; UAS-Arf1-dsRNA/UAS-InR-CFP*. C, G) *Cg-Gal4/+; UAS-Vps35-dsRNA/UAS-InR-CFP*. D, H) *Cg-Gal4/+; UAS-GRASP65-dsRNA/UAS-InR-CFP*.